Vol. 91 No. 2 pp. 581–601 ACTA GEOLOGICA SINICA (English Edition) Apr. 2017

Petrogenesis and Tectonics of the Naruo Porphyry Cu(Au) Deposit Related Intrusion in the Duolong Area, Central Tibet

DING Shuai[1], CHEN Yuchuan[2], TANG Juxing[2, *], ZHENG Wenbao[2], LIN Bin[3] and YANG Chao[4]

1 *College of Earth Sciences, Chengdu University of Technology, Chengdu 610059, China*
2 *Institute of Mineral Resources, Chinese Academy of Geological Sciences, Beijing 100037, China*
3 *CODES, ARC Centre of Excellence in Ore Deposits, University of Tasmania, Tasmania 7001, Australia*
4 *Department of Geology and Geological Engineering, Université Laval, Quebec City,G1V0A6, Canada*

Abstract: The Duolong area is the most important part of the Western Bangong-Nujiang Suture Zone porphyry Cu(Au) metallogenic belt, in Tibet, China. Here new detailed data are presented from LA-ICP-MS zircon U-Pb, whole-rock geochemical, and *in* -situ zircon Hf isotope analyses for igneous rocks in the large Naruo deposit (2.51 Mt of Cu and 82 t of Au) which is located ~2 km NE of the Duolong (Duobuza and Bolong) super-large gold-rich porphyry copper deposit. We integrated our results with previous research of other porphyry deposits in the Duolong area and have identified the timing, geodynamic setting, and petrogenesis of the mineralization-associated magmatic events. Based on the measurements, the Duolong area porphyry Cu(Au) deposit formations are associated with Early Cretaceous intermediate-felsic magmatism, which is consistent with U-Pb zircon ages of 120 Ma. All the main intrusive rocks in the ore-concentrated area have similar lithogeochemical characteristics; they show a relative enrichment in both light rare earth elements (LREEs) and large-ion lithophile elements (LILEs: Rb, Ba, K, etc.) and relative depletion in both heavy rare earth elements (HREEs) and high field strength elements (HFSEs: Nb, Ta, Zr, Hf, etc.). Moreover, the granite porphyry shows positive $\varepsilon Hf(t)$ values between 1.38–7.37 suggesting that magmas were potentially derived from the partial melting of a depleted mantle wedge that had been metasomatized by subducted slab-derived fluids or melts. This paper points out that the formation of the porphyry-epithermal Cu(Au) deposit in the Duolong area was dominated by northward subduction of the Bangongco Tethys Plate beneath the Qiangtang block in the Early Cretaceous (124–114 Ma), when the subducted oceanic crust reached 50–70 km underground and generated different degrees of phase transformation, which lead to a melt produced by dehydration of amphibole minerals, a metasomatized mantle wedge, and induced mantle partial melting that produced the magma. Those deposits occurred in a continental arc tectonic setting, which is similar to the continental margin arc environment of the ocean-continent subduction setting of the Andes metallogenic belt in South America.

Key words: geochemical signatures, zircon U-Pb, Hf isotope, Duolong area, continental arc, depleted mantle, Central Tibet, Proto-Tethys

1 Introduction

A porphyry deposit is one of the most economically important classes of mineral deposits of nonferrous metal resources (Gustafson, 1978; Sillitoe, 1979, 2010; Seedorff et al., 2005; Halter et al., 2005). They are also the main repositories of copper, molybdenum, and gold in the world (Richards, 2003; Cooke et a1., 2005; Singer, 2008; Kesler and Wilkinson, 2008; Sillitoe, 2010; Eliopoulos et al., 2014). They contain 80% of copper, 95% of molybdenum and more than 10% of gold in the world (Singer, 1995; Sinclair, 2007; Sun et al., 2013, 2015). Most of these deposits are parallel to magma arcs or orogenic belts and form in clusters (Richards, 2003; Sillitoe, 2010), such as the Canadian Cordillera belt (Logan and Mihalynuk, 2014), the Andes belt in South America (Sillitoe and Perelló, 2005), and the Apuseni-Banat-Timok-Srednogorie belt (Zimmerman et al., 2008). The Bangonghu Lake-Nujiang metallogenic belt, which is located in central

* Corresponding author. E-mail: tangjuxing@126.com

Tibet (Fig. 1a), is the third porphyry Cu(Au) belt(Li et al., 2011a, 2011b; Li et al., 2012; Qu Xiaoming et al., 2015) to be discovered after the Yulong (Hou et al., 2003, 2007; Jiang et al., 2008; Liang et al., 2009) and Gangdese belts (Hou et al., 2009; Tang et al., 2015; Zheng et al., 2015) (Fig. 1b). Many copper, iron, and gold deposits that are associated with porphyry are distributed to the north and south along this belt. Since the Duobuza and Bolong super-large porphyry Cu(Au) deposits (which together are called the Duolong deposit) were discovered in 2000, the No.5 Geological Team of the Bureau of Tibetan Geology and Exploration has found the Naruo large porphyry Cu (Au) deposit and the Rongna large porphyry-epithermal Cu(Ag-Au) deposit (which is also called the South Tiegelong deposit) in China recently (Tang Juxing et al., 2014; Yang Chao et al., 2014; Fang Xiang et al., 2015; Li Guangming et al., 2015). Together, these discoveries contain more than 2000 Mt of copper and over 300 t of gold (Duolong: 5.5 Mt of Cu and 180 t of Au; Rongna: 8.58 Mt of Cu and 28 t of Au; Naruo: 2.51 Mt of Cu and 82 t of Au; the characteristics of these deposits are listed in Table 1). The area is recognized as a giant metallogenic belt that is comparable to the Andes mineral belt in South America.

However, in contrast to the widely accepted opinion that the Yulong and Gangdese metallogenic belts formed in a post-collisional orogenic environment (Hou et al., 2007, 2009, 2013; Liang et al., 2006,2009; Zheng et al., 2015; Qu Huanhuan and Sun maoyu, 2016), the formation and origin of the Cu(Au) deposits in the Duolong area are still disputed. Previous detailed studies of the geochronology and geochemistry about these deposits resulted in different interpretations, including (1) these deposits formed during crustal uplift after the closure of the Bangong Lake-Nujiang Ocean basin, which was the product of thickened crustal melting (Qu Xiaoming et al., 2006, 2012, 2015; Qu et al., 2012; Xin Hongbo et al.,2009); (2) the island arc environment of the subduction zone of the Bangong Lake-Nujiang Tethys Ocean contain ore-bearing magma from the partial melting of the oceanic crust (Li Jinxiang et al., 2008; Li et al., 2011b, 2013; She Hongquan et al., 2009; Chen Huaan et al., 2013; Zhu

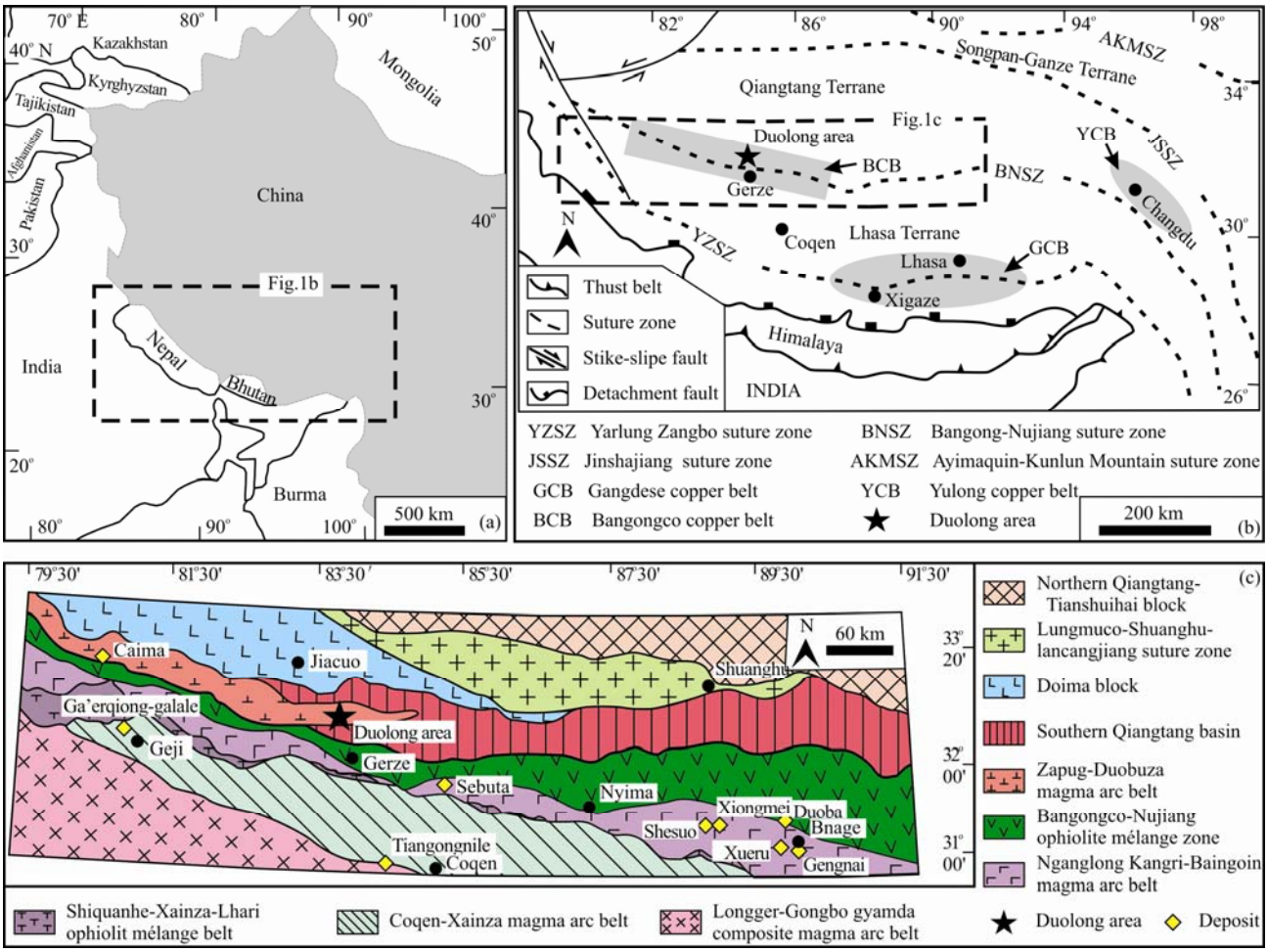

Fig. 1. (a) Geographic map of China; (b) sketch of a tectonic map of Tibet (modified after Hou et al., 2004); (c) tectonic units of the Bangong-Nujiang suture zone and its neighboring areas (modified after Geng Quanru et al., 2011).

Table 1 Geological characteristics of the deposits in the Duolong area

Deposit type	Typical deposit	Element	Reserves	Grade	Ore body type	Associate porphyry and age	Alteration	Ore minerals	Gangue minerals
Porphyry deposit	Naruo	Cu(Au)	Cu 2.51 Mt Au 82 t	Cu 0.38% Au 0.19 g/t	veinlet, disseminated and breccia	Early Cretaceous granodiorite porphyry (119.32–120.6 Ma)	potassic, sericitic, propylitic	pyrite, chalcopyrite, bornite, covellite, magnetite, hematite, molybdenite, galena, sphalerite	quartz, K-feldspar, plagioclase, biotite, sericite, chlorite, epidote, calcite
	Duobuza	Cu(Au)	Cu>3 Mt Au>90 t	Cu 0.51% Au 0.2 g/t	veinlet, disseminated	Early Cretaceous granodiorite porphyry (116.1–121.6 Ma)	potassic, sericitic, propylitic, intermediate argillic	chalcopyrite, pyrite, bornite, magnetite, molybdenite, native gold	quartz, K-feldspar, plagioclase, biotite, sericite, chlorite, epidote, illite, kaolinite
	Bolong	Cu(Au)	Cu>2 Mt Au>85 t	Cu 0.47% Au 0.22 g/t	veinlet, disseminated	Early Cretaceous granodiorite porphyry and quartz diorite porphyry (117.5–121.1Ma)	potassic, sericitic, propylitic, intermediate argillic	chalcopyrite, pyrite, bornite, magnetite, molybdenite, native gold	quartz, K-feldspar, plagioclase, biotite, sericite, chlorite, epidote, tourmaline, calcite, illite, kaolinite
High-sulphidation epithermal deposit	Rongna	Cu(Au,Ag)	Cu 8.56 Mt Au 28t Ag 2000 t	Cu 0.51% Au 0.13 g/t Ag 1.78 g/t	veinlet, disseminated and breccia	Early Cretaceous granodiorite porphyry (120.2 Ma)	potassic, phyllic, advanced argillic, quartz-alunite	covellite, digenite, chalcocite, enargite, chalcopyrite, bornite, pyrite	quartz, sericite, alunite, kaolinite, dickite, anhydrite, pyrophyllite
Low-sulphidation epithermal deposit	Nadun	Au(Cu)	Cu 0.3 Mt Au 1.7 t	Cu 0.75% Au 1.45 g/t	veinlet, breccia	Early Cretaceous granodiorite porphyry and quartz diorite porphyry (113–119 Ma)	sericitic, argillic, quartz-chalcedony-ad ularia-carbonates	chalcopyrite, pyrite, electrum, galena, sphalerite, bornite, cinnabar, wittichenite, cuprobismutite	quartz, chalcedony, adularia, sericite, calcite

Xiangping et al., 2015; Zhu et al., 2015; Fang Xiang et al., 2015); and (3) the deposits developed from the accretionary wedge on the continental margin, and both the oceanic crust and the accretionary wedge provided ore-forming materials (Li Guangming et al., 2011;Duan Zhiming et al., 2013).

Therefore, this paper focuses on the Naruo Cu(Au) deposit and the geochemistry of the granodiorite porphyry, zircon U-Pb dating, and the *in*-situ Hf isotopes. Compared the integrated results of previous research on other porphyry deposits in the Duolong area, this study identified magmatic events related to the mineralization, tectonic setting, and deep dynamic processes.

2 Geological Background and Ore Deposit Geology

2.1 Geological background

The Duolong area is located to the north of the Bangong-Nujiang suture zone junction in the Zapug-Duobuza magma arc in southern Qiangtang (Fig. 1c). The magma arc extends over 300 km from west of Ritu to north Gerze in southern Qiangtang and is thought to have formed due to the northward subduction of the Bangong Lake-Nujiang Tethys ocean during the Late Jurassic and the Early Cretaceous (Liao Liugen et al., 2005; Geng Quanru et al., 2011; Li et al., 2014). The Duolong area contains multiple porphyry-epithermal Cu(Au) deposits that are distributed along a deep fault (F10) that extends northeast to southwest (Fig. 2a). The formation of these deposits is associated with Early Cretaceous calc-alkali or high-potassium intermediate-felsic intrusions, including granodiorite porphyry, quartz diorite porphyry, quartz porphyry, and monzogranite porphyry. The strata in the area mainly consist of a sequence of continental volcanic rocks and littoral-facies sedimentary rocks. The sedimentary rocks include limestone of the Upper Triassic Rigan Peicuo Group (T_3r), feldspar quartz sandstone and slate of the Early Jurassic Quse Group (J_1q), sandstone and siltstone of the Middle-Late Jurassic Sewa Group ($J_{1\text{-}2}s$), and the conglomerate of the Oligocene Kangtuo Group, which unconformably covers the Mesozoic sedimentary system (Fig. 2a). This set of sedimentary formations is also defined as the southern Qiangtang accretionary wedge (Li Guangming et al., 2011). The volcanic rocks are dacite and andesite of the Early Cretaceous Meiriqiecuo Group and have a zircon U-Pb age of 110.01±0.7 Ma (Wang Qin et al., 2015), which is younger than the main ore-bearing porphyry in the area and are important protective layers against erosion. The deposit contains three main groups of faults, which have east-west, northeast, and northwest trends (Fig. 2a). The northeast and east-west faults control

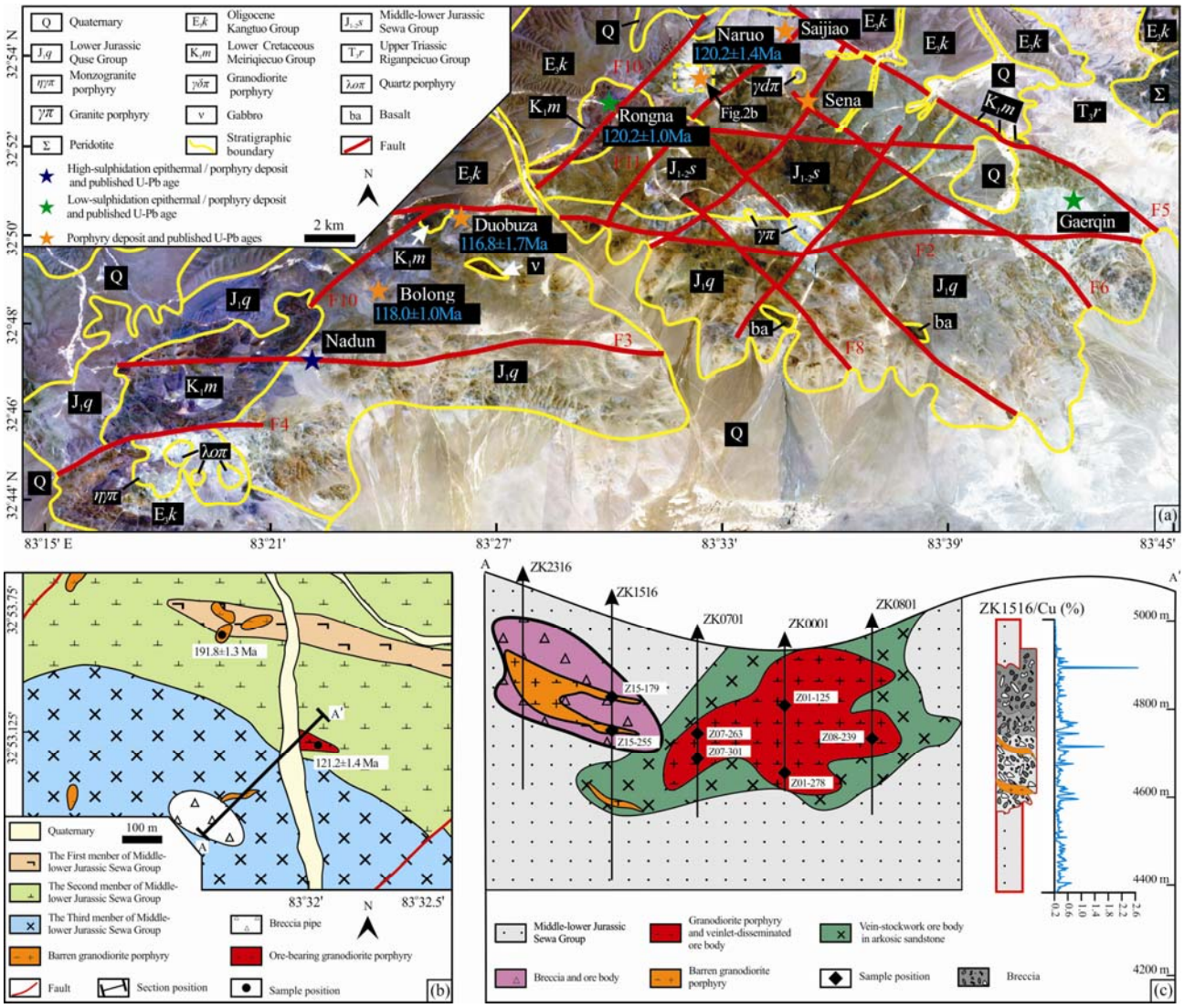

Fig. 2. (a) Geological map of Duolong area and Naruo porphyry Cu(Au) deposit (b); (c) Section A-A' of the Naruo deposit.
The published zircon U-Pb ages are from Li et al. (2011, 2013), Fang Xiang et al. (2014), Zhu Xiangping et al. (2015).

the rocks and the structure. Magma emplacement and the formation of the ore deposit occurred at the junction between the two groups of faults.

2.2 Ore deposit geology

The Naruo Cu(Au) deposit is located east of the Duolong deposits approximately 8 km from the southwestern Duolong super-large porphyry Cu(Au) deposit (Fig. 2a). It is a newly discovered large porphyry Cu(Au) deposit (Cu: 2.51 Mt @ 0.38%, Au: 82 t @ 0.19 g/t). The stratigraphy of this area is relatively simple; the main components are feldspar quartz sandstone and slate of the Middle-Late Jurassic Sewa Group and dacite and andesite of the Late Cretaceous Meiriqiecuo Group. In addition, a small amount of granodiorite porphyry is exposed in the northeast and southwest parts of the deposit (Fig. 2b), which have branch-like or vein-like shapes and intrude into the feldspar quartz sandstone of the Sewa Group. The granodiorite porphyry can be divided into two phases according to whether they bear ores. The early phase is exposed in the middle of the deposit and is the main ore-bearing porphyry for mineralization and alteration and has a zonal distribution around this intrusion (Fig. 2c). The late phase is exposed in the southwestern and northwestern parts of the deposit and does not show significant mineralization and alteration. The northeast-trending F10 and F11 faults pass through this area, with the F10 being the main ore-controlling structure.

The ore body in the Naruo deposit can be classified into three types, which are veinlet-disseminated in granodiorite porphyry, veins-stockwork in feldspar quartz sandstone, and cryptoexplosion breccia (Fig. 2c). The veinlet-disseminated ore body is located in the center of the deposit. The sulfides form star-like patterns in the

granodiorite porphyry with accompanying quartz sulfide veinlets (Fig. 3a,b). The vein-stockwork ore body in the sandstone is distributed around the porphyry and resulted from filling and metasomatism of hydrothermal fluid along gaps. The veins vary in width from 0.3 cm to 3 cm and are filled with several sulfides, such as pyrite, molybdenite, and chalcopyrite (Fig. 3c,d). The cryptoexplosion breccia ore body is located in the southwest part of the deposit and forms an upright cylinder. This body is 200 m long, 150 m wide and 30~150 m thick and may have formed because of deep magmatic activity. The main components of the breccia are feldspar quartz sandstone and granodiorite porphyry with triangular, platy, elliptical, or irregular shapes. The size of the breccia ranges from 0.5 cm to 10 cm, and it accounts for 50%–70% of the total volume of the breccia ore body (Fig. 3e). The matrix is mainly composed of quartz, calcite, chlorite, epidote, sericite and pyrite,

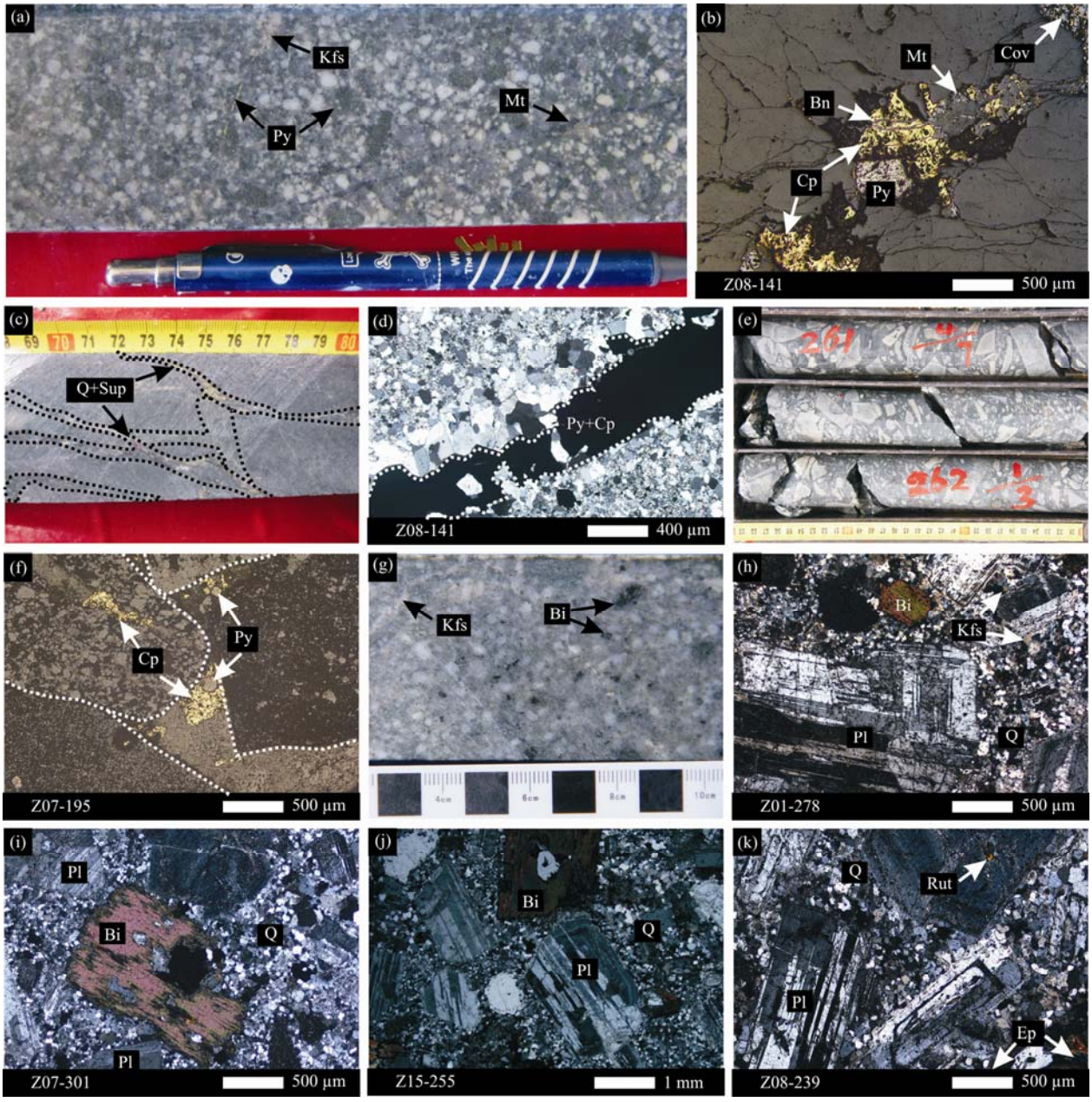

Fig. 3. Photographs of rocks, ore minerals, veins, and alterations in the Naruo porphyry Cu(Au) deposit.
(a) Porphyry ore body; (b) Disseminated minerals in granodiorite porphyry; (c) Vein-stockwork ore body in arkosic sandstone; (d) Sulphide-bearing quartz vein; (e) Breccia ore body; (f) Minerals between breccia clasts; (g) Ore-bearing granodiorite porphyry; (h) Ore-bearing granodiorite porphyry with little potassic alteration (Z0-278 sample was used for LA-ICP-MS zircon U-Pb and Hf isotope dating); (i) Ore-bearing granodiorite porphyry under polarized light; (j)Ore-bearing granodiorite porphyry under polarized light; (k),Barren granodiorite porphyry with little propylitc alteration (Z15-255 sample was used for LA-ICP-MS zircon U-Pb and Hf isotope dating). Py, Pyrite; Mt, magnetite; Cp, chalcopyrite; Bn, bornite; Cov, covellite; Sup, Sulphide; Q, quartz; Kfs, K-feldspar; Pl, plagioclase; Bi, biotite; Ep, epidote; Rut, rutile.

chalcopyrite, and hematite with small amounts of galena and sphalerite (Fig. 3f).

The metallic minerals in this deposit are chalcopyrite, pyrite, magnetite, hematite with small amounts of molybdenite, galena, sphalerite, covellite, and associated gold. The mineralization of these minerals is related to potassic alteration, silicification, sericitic alteration, chlorite, and epidotization. In addition, different types of alteration have converted the porphyry body at the center gradually from potassic zone to phyllic alteration, and shallow propylitization zone. However, argillization is not present in this deposit. Four periods of mineralization were identified based on the mineral compositions; from early to late, the periods are quartz-feldspar-biotite-chalcopyrite-pyrite-magnetite, quartz-pyrite-sericite-chalcopyrite, quartz-chlorite-epidote-pyrite-hematite, and quartz- molybdenite.

3 Sampling and Petrography

Fresh ore-bearing granodiorite porphyry samples were collected from boreholes of lines 0, 7 and 8 in the Naruo deposit (No. Z01-125, Z01-278, Z07-263, Z07-301, and Z08-239). Barren granodiorite porphyry samples were collected from borehole of line 15 (Z15-179 and Z15-255). ZK01-278 and ZK15-255 were selected as representatives of the ore-bearing and barren granodiorite porphyryfor the zircon U-Pb dating and Hf isotope analysis.

All of the samples have porphyritic textures (Fig. 3g). The phenocrysts of ore-bearing granodiorite porphyry are composed of 22%–28% quartz, 30%–40% plagioclase, 7%–15% K-feldspar, 15%–20% biotite, and 5%–8% amphibole (Fig. 3h, i, j). The main components of the matrix are fine-grained feldspar, quartz, chlorite, epidote, sericite, and some accessory minerals of apatite, sphene, zircon, rutile, and magnetite. Strong potassic alteration and weak chloritization occured (Fig. 3h, i, j). In contrast to the ore-bearing granodiorite porphyry, K-feldspar and magnetite were very rare (3%–5%) in the barren granodiorite porphyry. The formation of chlorite and epidote is strong, while potassic alteration is weak (Fig. 3k).

4. Analytical Methods

4.1 Major and trace element analysis

The whole-rock major and trace elements were measured at the Southern Institute of Metallurgy and Geological Testing. The major elements were tested using an X-ray fluorescence spectrometer. After being crushed, shrunk, and weighed, the samples were melted with anhydrous lithium tetraborate. Ammonium nitrate was used as the oxidant, and lithium fluoride and a small amount of lithium bromide were used as the flux and mold-release agents. The samples were then made into glass slices. Finally, the samples were measured using an Axios X-ray fluorescence spectrometer (PANalytical Company, Netherlands). The measurement error of each element was less than 1%. The trace elements were measured by Inductively Coupled Plasma Mass Spectrometry (ICP-MS). The ground samples were melted by tetraborate and then analyzed using a NexION 300x plasma mass spectrometer (PE Company, USA). The measurement error of each element was less than 1%.

4.2 Zircon U–Pb

The granodiorite porphyry samples that were used for the zircon U-Pb dating and Hf isotope analysis were sent to the lab to select the zircons and make the targets. The selection of single zircons was conducted in the Institute of Regional Geological Survey, Hebei Institute of Geological Survey, Langfang, Hebei, China. Crystalline zircons were selected from each sample under a binocular microscope and then stuck in double-faced adhesive tape and stabilized with colorless, transparent epoxy resin. After the epoxy resin was fully hardened, the surfaces of the target zircons were polished, and the interiors were fully exposed. The target zircons were sent to the Institute of Mineral Resources at the Chinese Academy of Geological Sciences for cathode luminescence with a JXA2800 Electron microprobe. The zircons with good crystals and well-developed zones were selected and sent to the Isotope Testing Laboratory at the Tianjin Institute of Geology and Mineral Resources for U-Pb dating using the LA-ICP-MS method (Fig. 4). The instruments for the U-Pb dating included a Neptune Mass Spectrometer (Thermo Fisher, USA) and a UP193-FX Ar F Excimer laser (ESI Company, USA) with a laser beam spot diameter of 35 μm, a frequency of 8–10 Hz, and a laser energy density of 13–14 J/cm^2. To ensure that U-Pb with large differences in mass would be simultaneously accepted, the isotope testing laboratory used a dynamic zooming and dispersion method. A single point erosion method was used to collect the samples. After the completion of sample testing and age calculation for every 4–5 samples, TEMORA was used as an age standard for the exterior of the zircons. The Isoplot programs (Ludwig, 2003) were used for the data processing. Common lead correction was conducted following the data processing method of Andersen (2002). After the testing was complete, NIST612 was used as an external standard to calculate the Pb, U, and Th contents of the zircon samples to guarantee that the results were accurate and reliable.

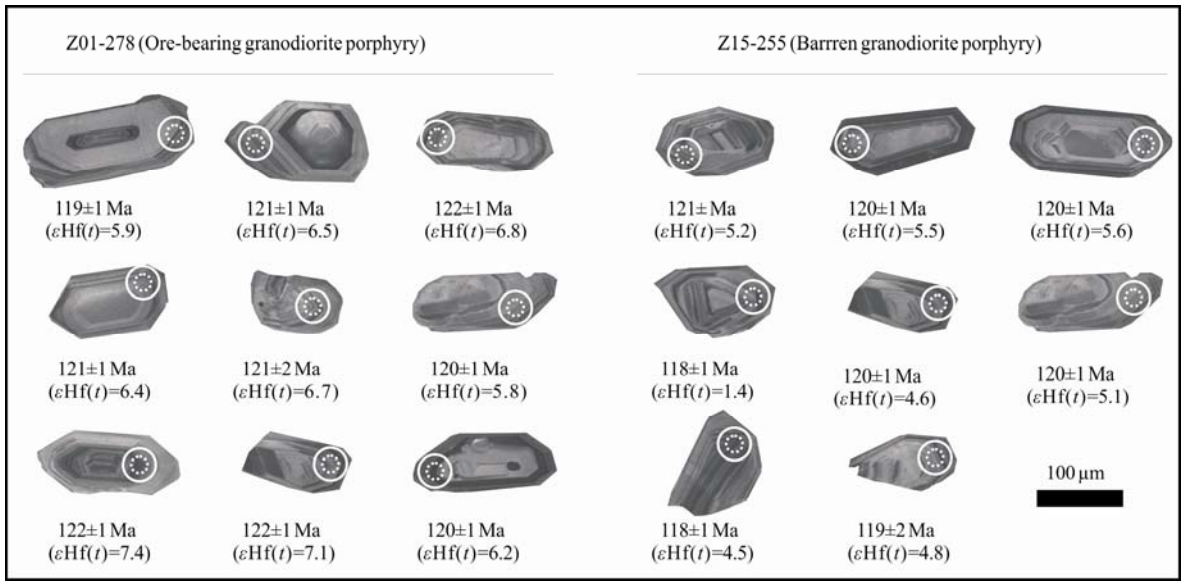

Fig. 4. Zircon (CL) images with analysis spots, U-Pb ages, and $\varepsilon Hf(t)$ values from the Naruo porphyry Cu(Au) deposit.

4.3 Hf isotope analysis

The zircon in-situ isotope analysis was performed based on the U-Pb dating and tested the same dating points (Fig. 4). The testing was performed in the Key Laboratory of Metallogeny and Mineral Assessment at the Institute of Mineral Resources, Chinese Academy of Geological Sciences, with a Neptune Laser Ablation ICP-MS. He gas was used as the carrier gas for the erosion substances, and the diameter of the laser beam spot was 55 mm. The international GJ1 standard zircon was used as the reference standard. The instrument settings and the detailed testing procedures followed those of Hou Kejun et al. (2007). In the data analysis, the decay constant for ^{176}Lu was 1.867×10^{-11} a^{-1} (Söderlund et al., 2004). The chondrite ratios $n(^{176}Hf)/n(^{177}Hf) = 0.282772$ and $n(^{176}Lu)/n(^{177}Hf) = 0.0332$, which were recommended by Bouvier et al. (2008), were adopted to calculate the value of $\varepsilon Hf(t)$. Depleted mantle ratios of $n(^{176}Hf)/n(^{177}Hf) = 0.28325$ and $n(^{176}Lu)/n(^{177}Hf) = 0.015$ were used to calculate the Hf ages (Amelin et al., 1999). The weighted average of $^{176}Hf/^{177}Hf$ for the GJI zircon standard is 0.282003 ±0.000018 (n = 7), and the error is consistent with values from the literature (Hou Kejun et al. 2007).

5 Results

5.1 Zircon U-Pb age

Based on their cathode luminescence images, many of the granodiorite porphyry samples that were used for dating had long columnar shapes, and a few had granular and irregular shapes. The particle sizes ranged from 50 μm to 150 μm. Many particles had a good degree of self-formation and had relatively well-developed cylinders and cones. They also had clear oscillatory zoning, no internal residuals, and no metamorphosed edges (Fig. 4). The Th/U values were high (Table 2), which suggests that they were magmatic zircons (Belousova et a1., 2002), therefore, the ages that were measured by the zircon U-Pb dating represent the ages of magmatic crystallization.

Zircon particles from 12 sites in the ore-bearing granodiorite porphyry were tested (Table 2). The $^{206}Pb/^{238}U$ ages ranged from 122.1 Ma to 118.79 Ma, and the weighted average age was 120.63±0.55 Ma (MSWD=1.16)(Fig. 5a,b), which is consistent with a previous study that reported a zircon U-Pb age of 120.2±1.4 Ma (Zhu Xiangping et al., 2015). In addition, zircon particles from 11 sites in the barren granodiorite porphyry were tested (Table 2). The $^{206}Pb/^{238}U$ ages were between 117.96 Ma and 121.21 Ma (Table 2), and the weighted average age was 119.32±0.72 Ma (MSWD=1.4) (Fig. 5c,d), which is consistent with the age of 119.8±1.3 Ma that was obtained by Zhu Xiangping et al. (2015) and little younger than the age of the ore-bearing granodiorite porphyry. Therefore, the ore-bearing granodiorite porphyry and barren granodiorite porphyry belong to different phases of the same period.

5.2 Major and trace elements

Table 3 shows the results of the geochemical analysis of the granodiorite porphyry in the Naruo deposit. These magmatic rocks were generally enriched in silicon (SiO_2=63.91–65.54wt%) and potassium (K_2O = 2.25–4.6wt%) but were deficient in magnesium (MgO = 1.57–1.74wt%), titanium (TiO = 0.32–0.39wt%), phosphorus (P_2O_5 = 0.1–0.15wt%), and peraluminous (A/CNK = 1.69–2.3). The K_2O-SiO_2 and A/NK-A/CNK diagrams

Table 2 LA-ICM-MS zircon U–Pb isotope data of the granodiorite porphyry from the Naruo Cu(Au)deposit

Sample spots	Pb	Th	U	Th/U	Isotopic ratio						Age (Ma)					
	ppm				$^{206}Pb/^{238}U$	1σ	$^{207}Pb/^{235}U$	1σ	$^{207}Pb/^{206}Pb$	1σ	$^{206}Pb/^{238}U$	1σ	$^{207}Pb/^{235}U$	1σ	$^{207}Pb/^{206}Pb$	1σ
Z01-01	5	162	255	0.63	0.0187	0.0002	0.1443	0.0123	0.0560	0.0048	119.34	1.05	137	12	453	189
Z01-02	9	265	469	0.57	0.0186	0.0001	0.1553	0.0076	0.0606	0.0030	118.79	0.80	147	7	623	105
Z01-03	10	293	505	0.58	0.0189	0.0001	0.1252	0.0063	0.0479	0.0024	120.96	0.77	120	6	95	118
Z01-04	7	227	321	0.71	0.0188	0.0001	0.1350	0.0098	0.0520	0.0038	120.30	0.87	129	9	285	165
Z01-05	3	82	164	0.50	0.0187	0.0002	0.1395	0.0204	0.0540	0.0081	119.59	1.47	133	19	372	336
Z01-06	6	186	304	0.61	0.0188	0.0001	0.1413	0.0077	0.0544	0.0029	120.36	0.89	134	7	387	121
Z01-07	5	123	233	0.53	0.0189	0.0001	0.1605	0.0131	0.0615	0.0050	120.92	0.93	151	12	656	174
Z01-08	9	308	413	0.75	0.0190	0.0001	0.1752	0.0081	0.0669	0.0029	121.24	0.94	164	8	836	90
Z01-09	4	113	205	0.55	0.0190	0.0003	0.1300	0.0307	0.0496	0.0119	121.35	1.73	124	29	176	558
Z01-10	5	124	229	0.54	0.0191	0.0002	0.1293	0.0176	0.0492	0.0068	121.69	1.08	123	17	157	323
Z01-11	8	193	391	0.49	0.0191	0.0001	0.1267	0.0106	0.0482	0.0038	121.82	0.89	121	10	108	188
Z01-12	3	98	159	0.62	0.0191	0.0002	0.1380	0.0185	0.0523	0.0072	122.10	1.18	131	18	300	313
Z15-01	10	387	503	0.77	0.0185	0.0001	0.1412	0.0058	0.0555	0.0022	117.96	0.79	134	5	431	88
Z15-02	6	219	297	0.74	0.0185	0.0001	0.1467	0.0106	0.0575	0.0042	118.14	0.88	139	10	512	160
Z15-03	8	301	429	0.70	0.0185	0.0001	0.1304	0.0059	0.0510	0.0023	118.33	0.78	124	6	243	104
Z15-04	6	170	286	0.60	0.0188	0.0002	0.1400	0.0103	0.0540	0.0038	120.02	0.97	133	10	372	159
Z15-05	10	145	521	0.28	0.0187	0.0003	0.2119	0.0193	0.0824	0.0064	119.13	1.84	195	18	1255	152
Z15-06	11	450	528	0.85	0.0188	0.0001	0.1408	0.0063	0.0542	0.0024	120.31	0.79	134	6	380	99
Z15-07	5	150	251	0.60	0.0190	0.0001	0.1270	0.0105	0.0485	0.0040	121.21	0.92	121	10	126	193
Z15-08	4	109	214	0.51	0.0188	0.0002	0.1260	0.0186	0.0486	0.0074	120.02	1.07	121	18	130	357
Z15-09	3	80	159	0.50	0.0188	0.0002	0.1322	0.0174	0.0510	0.0070	120.00	1.12	126	17	242	316
Z15-10	8	179	441	0.41	0.0186	0.0001	0.1342	0.0084	0.0523	0.0032	118.87	0.79	128	8	299	140
Z15-11	14	565	689	0.82	0.0187	0.0001	0.1146	0.0043	0.0444	0.0016	119.63	0.90	110	4	–90	90

Note: use the $^{206}Pb/^{238}U$ age when the age < 1000 Ma, rather than using $^{207}Pb/^{206}Pb$ age.

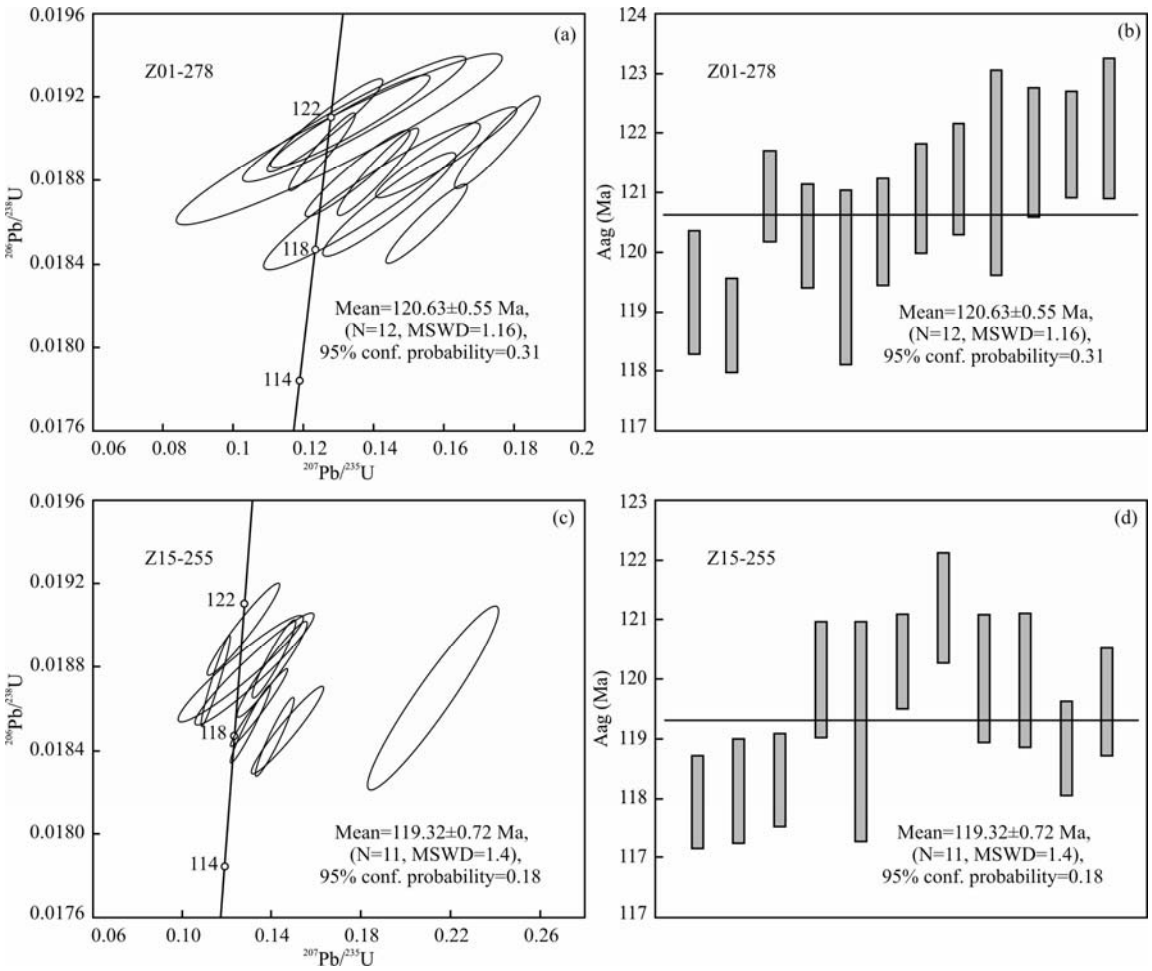

Fig. 5. Zircon U-Pb concordia diagrams and weighted mean $^{206}Pb/^{238}U$ages of thegranodiorite porphyry from the Naruo Cu(Au) deposit.

Table 3 Geochemical data for the granodiorite porphyry from the Naruo Cu(Au) deposit

Sample	Z01-125	Z01-278	Z07-263	Z07-301	Z08-239	Z15-179	Z15-255
Lithology	Ore-bearing granodiorite porphyry					Barren granodiorite porphyry	
Major element (wt%)							
SiO_2	65.01	65.13	64.53	65.54	64.85	63.91	64.71
Al_2O_3	15.19	14.16	15.98	15.87	15.45	15.50	14.96
Fe_2O_3	1.66	2.75	2.89	2.83	2.19	2.33	2.22
FeO	4.29	3.17	3.02	2.44	3.82	4.19	3.84
MgO	1.57	1.65	1.71	1.62	1.66	1.74	1.73
CaO	3.00	2.00	2.82	1.48	3.05	3.86	3.60
Na_2O	2.53	0.11	2.69	2.01	2.29	2.72	2.70
K_2O	3.01	4.60	2.64	3.44	2.80	2.61	2.25
TiO_2	0.37	0.36	0.37	0.32	0.38	0.39	0.38
MnO	0.14	0.19	0.07	0.07	0.09	0.08	0.09
P_2O_5	0.13	0.12	0.14	0.10	0.12	0.15	0.13
$Mg^{\#}$	32.6	34.27	35.15	36.68	33.84	33.06	34.56
LOSS	2.55	4.34	2.57	3.46	2.67	2.17	2.73
Total	99.45	98.57	99.44	99.17	99.37	99.64	99.34
ANK	2.05	2.74	2.19	2.26	2.27	2.18	2.13
ACNK	1.18	1.61	1.29	1.63	1.25	1.12	1.08
Trace element (ppm)							
Bi	0.70	2.21	0.22	0.52	0.48	0.22	0.10
Li	28.30	25.05	30.46	23.76	21.51	24.58	27.53
Be	1.46	1.09	1.36	1.25	1.30	1.17	1.33
Sc	8.97	7.07	8.25	7.81	8.03	7.16	7.71
V	81.62	59.88	76.13	87.61	82.01	74.19	83.80
Cr	7.34	4.78	5.77	5.05	6.03	6.18	7.23
Co	9.33	7.53	6.22	6.05	8.09	8.35	8.80
Ni	5.96	4.62	3.83	2.69	6.54	7.33	13.19
Cu	602.00	5733.00	399.30	357.30	1422.00	2528.50	356.30
Pb	12.57	10.44	9.44	6.07	10.67	10.75	8.76
Zn	110.05	77.25	60.87	50.05	64.84	67.41	38.05
Ga	18.04	15.62	18.27	18.09	17.56	17.99	18.16
Rb	72.32	193.70	75.71	133.10	90.12	63.51	90.49
Sr	421.40	421.7	402.70	208.20	379.30	453.85	480.90
Y	12.07	7.99	12.57	12.84	8.93	9.35	9.59
Zr	95.18	76.82	91.61	84.08	97.41	97.92	89.95
Nb	8.81	6.59	5.26	5.27	7.29	6.78	7.88
Cs	18.32	17.71	16.62	15.98	10.99	10.92	28.79
Ba	615.70	791.20	515.70	591.30	425.90	414.60	482.50
La	12.60	9.33	10.60	15.44	8.74	10.60	10.72
Ce	18.72	15.42	16.19	25.60	12.59	15.30	15.64
Pr	2.84	2.35	2.60	3.89	1.89	2.26	2.29
Nd	11.28	9.27	10.86	15.56	7.61	9.03	9.07
Sm	2.19	1.88	2.20	2.96	1.47	1.74	1.73
Eu	0.60	0.69	0.63	0.81	0.51	0.57	0.58
Gd	1.88	1.86	1.96	2.71	1.40	1.59	1.59
Tb	0.35	0.35	0.37	0.50	0.26	0.28	0.28
Dy	1.90	1.98	2.08	2.71	1.41	1.55	1.52
Ho	0.35	0.32	0.38	0.47	0.26	0.29	0.28
Er	1.18	1.09	1.26	1.56	0.84	0.92	0.90
Tm	0.19	0.17	0.20	0.27	0.13	0.14	0.14
Yb	1.31	1.11	1.38	1.62	0.86	0.90	0.90
Lu	0.21	0.17	0.22	0.26	0.14	0.15	0.14
Hf	12.07	7.99	12.57	12.84	8.93	9.35	9.59
Ta	0.76	0.57	0.48	1.00	0.52	0.53	0.71
Tl	0.84	1.65	0.88	1.08	1.09	0.85	1.31
Th	9.93	9.06	8.07	6.76	6.59	7.07	7.36
U	1.12	0.88	0.87	0.75	0.37	0.49	0.64
ΣREE	55.57	45.99	50.93	74.38	38.10	45.32	45.79
LREE	48.22	38.93	43.07	64.28	32.81	39.50	40.03
HREE	7.35	7.06	7.86	10.10	5.29	5.82	5.76
LREE/HREE	6.56	5.52	5.48	6.37	6.20	6.79	6.95
δEu	0.91	1.14	0.93	0.88	1.09	1.05	1.07
δCe	0.77	0.81	0.76	0.81	0.76	0.77	0.77
La_N/Yb_N	6.91	6.04	5.53	6.84	7.28	8.41	8.54

Note: A/CNK=$(Al_2O_3)/(CaO + K_2O + Na_2O)$ molar ratio; A/NK=$(Al_2O_3)/(K_2O + Na_2O)$ molar ratio; $\delta Eu=Eu_N/[(Sm_N)\times(Gd_N)]^{1/2}$; $\delta Ce=Ce_N/[(La_N)(Pr_N)]^{1/2}$.

indicate that most of the samples belong to a high potassium calc-alkaline and peraluminous rock series (Figs. 6a, b). However, the ore-bearing granodiorite porphyry had higher SiO_2, K_2O, and A/CNK contents, which is consistent with early data from the Duolong and Naruo deposits and suggests that the mineralization may be closely related to

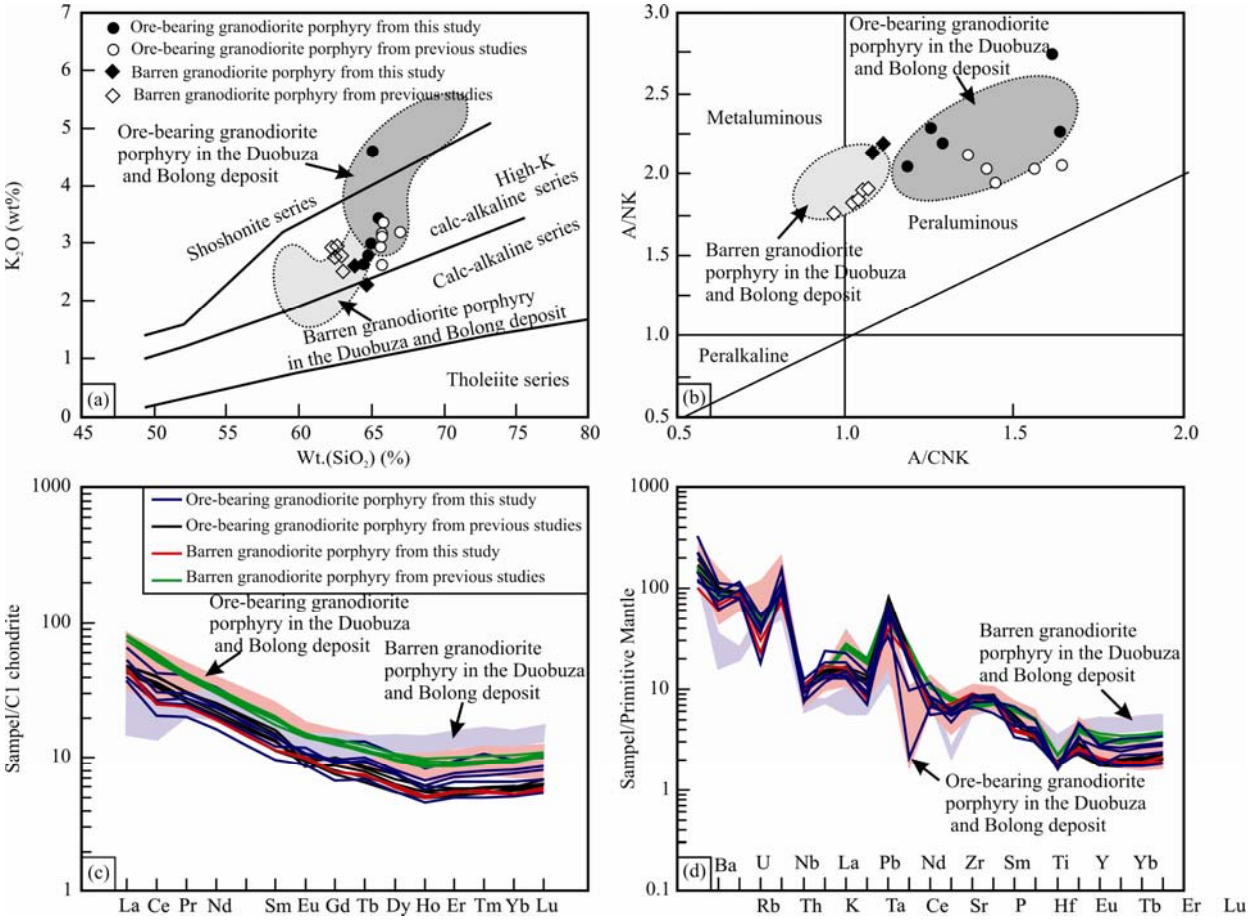

Fig. 6. Geochemical diagram of granodiorite porphyry from the Naruo porphyry Cu (Au) deposit.
(a) SiO_2 versus K_2O; (b) A/CNK (mole $[Al_2O_3/(CaO+Na_2O+K_2O)]$) versus A/NK (mole $[Al_2O_3/(Na_2O+K_2O)]$) (after Peccerillo and Taylor, 1976); (c) Cl-chondrite-normalized rare earth element patterns; (d) primitive mantle-normalized trace element spidergrams. C1-chondrite and primitive mantle values are taken from Boynton (1984) and Sun and McDonough (1989), respectively. The data for the ore-bearing and barren granodiorite porphyry in the Duobuza and Bolong deposit are from Li et al. (2013); Chen Huaan et al. (2013). The data for the published granodiorite porphyry are from Zhu Xiangping et al. (2015).

potassic alteration and silicification. All of the rocks were relatively enriched in light rare earth elements (SLREE/SHREE = 5.48–6.95) and large-ion lithophile elements (LILEs; e.g., Rb, K, Sr) and low in heavy rare earth elements (HREEs; La_N/Yb_N = 5.53–8.54) and high field strength elements (HFSEs; e.g., Nb, Ta, Ti, P). In addition, the rocks had a weakly negative Ce anomaly and no Eu anomaly (Figs. 6c, d). Compared with early studies of the Duolong and Naruo deposits, this study showed that the ore-bearing granodiorite porphyry had a higher HREE than the barren granodiorite porphyry, but all had the geochemical characteristics of arc magmas in a subduction zone setting (Rollinson, 1993; Stolz et al., 1996; Grove et al. 2003).

5.3 *in*-situ Hf isotope analysis of zircon

Table 4 shows the results of the zircon Hf isotope analysis of the granodiorite porphyry in the Naruo deposit. Of the nine samples of the granodiorite porphyry that were tested (Z01), the initial values of $^{176}Hf/^{177}Hf$ varied between 0.282863 and 0.282906, $\varepsilon Hf(t)$ ranges from 5.77 to 7.37 (Fig. 7a), and the two-stage model ages (TDMC) were between 707 Ma and 808 Ma. The barren granodiorite porphyry had lower values of $^{176}Hf/^{177}Hf$ and $\varepsilon Hf(t)$, which were 0.28274–0.28286 and 1.38–5.63 (Fig. 7b), respectively. The two-stage model ages were between 816 Ma and 1086 Ma, which is consistent with previous reports and suggests that much more crustal material was mixed during the late period of the formation of the barren granodiorite porphyry (Zhu Xiangping et al., 2015).

6 Discussions

6.1 Magmatic event in the Duolong area

The zircon U-Pb age of the granodiorite porphyry measured is 19–120 Ma in this research. In addition, the Re-Os model ages of two molybdenite crystals are 116.6 ± 2.6 Ma and 118.5±2.2 Ma (another article), the metallogenic age corresponds to the emplacement timing of granodiorite porphyry, which indicates that the formation of

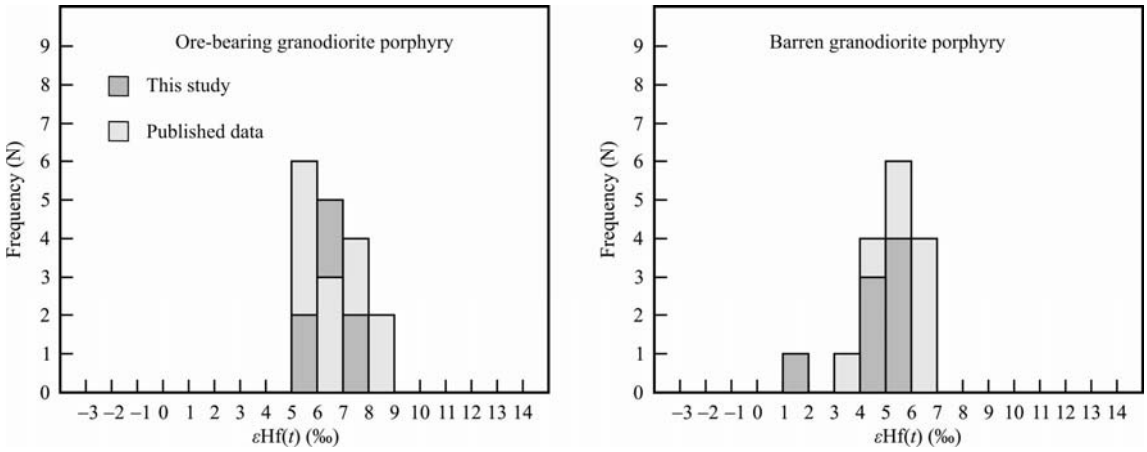

Fig. 7. Frequency histogram of zircon $\varepsilon Hf(t)$ values from the Naruo porphyry Cu(Au) deposit.
The published data are from Zhu Xiangping et al. (2015).

Table 4 Hf isotopes analyzed data of the zircons from the Naruo Cu(Au) deposit

Lithology	Sample No.	Age (Ma)	$^{176}Yb/^{177}Hf$	$^{176}Lu/^{177}Hf$	$^{176}Hf/^{177}Hf$	2σ	$^{176}Hf/^{177}Hf_i$	$\varepsilon_{Hf}(0)$ (‰)	$\varepsilon_{Hf}(t)$ (‰)	2σ	T_{DM} (Ma)	T_{DM}^C (Ma)	$f_{Lu/Hf}$
Ore-bearing granodiorite porphyry	Z01-01	119.59	0.062560	0.001861	0.282868	0.000016	0.282864	3.39	5.87	0.6	558	801	−0.94
	Z01-02	121.24	0.035551	0.001092	0.282883	0.000016	0.282881	3.94	6.51	0.6	524	761	−0.97
	Z01-03	121.69	0.059476	0.001616	0.282893	0.000014	0.282890	4.29	6.83	0.5	517	741	−0.95
	Z01-04	120.92	0.047134	0.001418	0.282881	0.000015	0.282878	3.85	6.39	0.5	532	768	−0.96
	Z01-05	121.35	0.052565	0.001445	0.282889	0.000016	0.282886	4.13	6.68	0.6	521	750	−0.96
	Z01-06	120.30	0.034450	0.001024	0.282863	0.000015	0.282860	3.21	5.77	0.5	553	808	−0.97
	Z01-07	122.10	0.026299	0.000772	0.282906	0.000016	0.282905	4.75	7.37	0.6	487	707	−0.98
	Z01-08	121.82	0.031657	0.000958	0.282899	0.000013	0.282897	4.50	7.09	0.5	500	724	−0.97
	Z01-09	120.36	0.054250	0.001642	0.282876	0.000013	0.282872	3.67	6.18	0.5	543	781	−0.95
Barren granodiorite porphyry	Z15-01	121.21	0.029555	0.000831	0.282846	0.000017	0.282845	2.63	5.23	0.6	573	843	−0.97
	Z15-02	120.02	0.019530	0.000565	0.282853	0.000014	0.282852	2.88	5.47	0.5	559	827	−0.98
	Z15-03	120.00	0.047284	0.001260	0.282860	0.000016	0.282857	3.10	5.63	0.6	561	816	−0.96
	Z15-04	118.14	0.032316	0.000841	0.282740	0.000016	0.282738	-1.15	1.38	0.6	724	1086	−0.97
	Z15-05	120.02	0.031431	0.000879	0.282830	0.000015	0.282828	2.05	4.62	0.5	597	881	−0.97
	Z15-06	120.31	0.034790	0.000999	0.282844	0.000015	0.282842	2.54	5.10	0.5	579	851	−0.97
	Z15-07	118.33	0.033119	0.000980	0.282829	0.000016	0.282827	2.01	4.53	0.6	600	885	−0.97
	Z15-08	119.13	0.032367	0.001021	0.282835	0.000015	0.282833	2.23	4.77	0.5	592	871	−0.97

the Naruo depositwas related to the magmatic hydrothermal activity that resulted from the emplacement of the granodiorite porphyry. Combined with previously published ages for U-Pb analyses of zircons, the Re-Os age of molybdenite and $^{40}Ar/^{39}Ar$ analyses (She Hongquan et al., 2009; Li Jinxiang et al., 2008; Li et al., 2011a, 2011b, 2013; Fang Xiang et al., 2015; Chen Huaan et al., 2013; Zhu et al., 2015; Wang Qin et al., 2015). She Hongquan et al. (2009) reported 120.9±2.4 Ma for the ore-bearing granodiorite porphyry and an isochron age 118.0±1.5Ma of molybdenite from the Duobuza deposit. Li et al. (2011) reported the $^{40}Ar/^{39}Ar$ age of 115.2±1.1 Ma from the hydrothermal K-feldspar and 115.2±1.2 Ma from the sericite, which show a close temporal relationship of the ore-bearing granodiorite porphyry in the Duobuza deposit. Furthermore, Chen Huaan et al. (2013) reported a 119–120 Ma zircon age for the Bolong deposit, Zhu Xiangping et al. (2015) reporteda zircon U-Pb age of 120 Ma from the Naruo deposit, and Fang Xiang et al. (2015) obtained 120.2±1.0 Ma for ore-bearing porphyry and an isotopic model age of 118.45±0.76 Ma of molybdenite in the Rongna deposit. All the data indicate that the large-scale intermediate-felsic magmatic activity during the Early Cretaceous (124–114 Ma) was the major factor in the formation of the porphyry-epithermal Cu(Au) deposit in the Duolong area, and the magmatic activity in this area was concentrated in three phases (Fig. 8). The granodiorite porphyry contains the major intrusive rocks of the first phase that are related to mineralization. The second and third phases were marked by large amounts of volcanic rocks (including andesite, basaltic andesite) that covered the early intrusive rocks at 113–108 Ma and 107–104 Ma, respectively.

6.2 Tectonic implication

Although many researchers believe that the large-scale magmatic activity in the Duolong area was related to the subduction of the Bangong Lake-Nujiang Tethys ocean basin(Liao Liugen et al., 2005; Cao Shenghua et al., 2006; Geng Quan ru et al., 2011; Li et al., 2014), there are still many controversial issues about this theory, such as did it form during subduction(Li et al., 2011b, 2013; Fang Xiang et al., 2015; Zhu et al., 2015) or after the collision of the Lhasa and Qiangtang terranes (Qu Xiaoming et al., 2006,

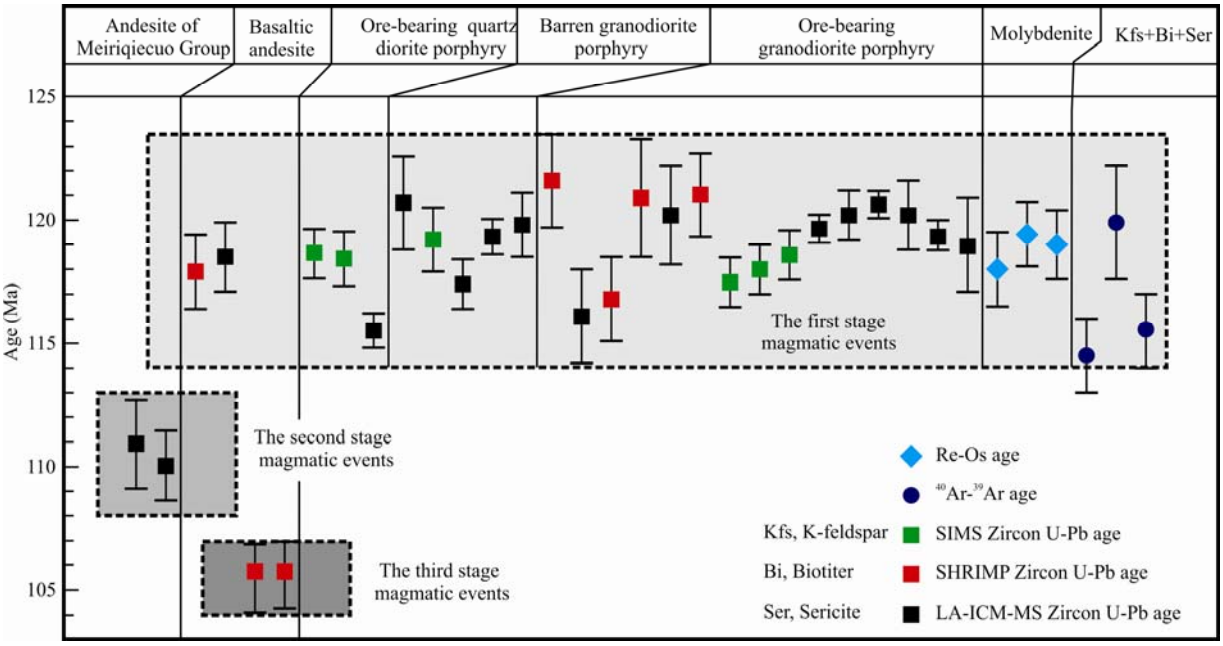

Fig. 8. Age of main magmatic events in the Duolong area. (35 age data points from the five deposits of Duobuza, Bolong, Naruo porphyry deposit, and Nadun and Rongna epithermal deposits).
Data sources quoted from She Hongquan et al. (2009), Li Jinxiang et al.(2008), Li et al. 2011a, 2011b, 2013), Fang Xiang et al. (2015), Chen Huaan et al. (2013), Zhu Xiangping et al. (2015), Wang Qin et al. (2015). This suggests that the first stage is 124–114 Ma, the second stageis 113–108 Ma, and, the third stage is 107–104 Ma.

2012, 2015; Qu et al., 2012; Xin Hongbo et al., 2009)? Did the island arc environment form by intra-ocean subduction (Liu et al., 2014) or in a continental margin arc environment above an ocean-continent subduction (Li et al., 2011b, 2013, 2014; Zhou Jinsheng et al., 2013)? The key question is the evolution of the Bangong Lake-Nujiang Tethys Ocean in the Early Cretaceous. Previous studies have shown that the Bangong Lake-Nujiang Tethys Ocean started to subduct to the north during the Middle-Late Jurassic (177.1–150 Ma) (Shi Rendeng, 2007; Qu Xiaoming et al., 2009), and was accompanied by intra-oceanand ocean-continent subduction, which formed island arc magmatic rocks in the Bangong Lake-Nujiang River (Matte et al., 1996; Liu et al., 2014) and continental margin arc magmatic rocks to the south of Qiangtang(Li et al., 2014; Liu et al., 2012; Guynn et al., 2006; Schwab et al., 2004). However, there are several opinions about the timing of the closure of the Bangong Lake-Nujiang Tethys Ocean. Qu et al. (2012) obtained an age of 109.6–113.7 Ma for A-type granite in the middle of the Bangong Lake-Nujiang River and defined the timing of the closure of the ocean basin as the Early Cretaceous at approximately 145 Ma, which is consistent with the results of previous studies (Kapp et al., 2003; Yin and Harrison, 2000). Therefore, some researchers believed that the magmatic rocks in the Duolong area formed after the collision of the Lhasa and Qiangtong terranes(Qu Xiaoming et al., 2006, 2012, 2015; Qu et al., 2012; Xin Hongbo et al., 2009). However, a lot of excellent research has been carried out on the strata structure and magmatic activities at the South Qiangtang terrane in recent years and more scholars believe that the closure time of the Bangong Lake-Nujiang Tethys Ocean may extend to the late Early Cretaceous (Liu et al., 2014; Li et al., 2015; Zhou Xiong et al., 2015). For example, Zhu Dicheng et al. (2006) point out that the Bangong Lake-Nujiang Tethys oceanic crust has not yet completely closed in the late Early Cretaceous of about 110Ma based on the zircon age of oceanic island basalt from the Doima and Tarenben area in the Bangong-Nujiang suture belt. Li Dewei. (2008) considered that the unconformablestrata of the late Early Cretaceous Jingjishan and Yuduo group are a sign of Tethys ocean-land conversion. Moreover, Zhang Shuo et al. (2014) and Fu Jiajun et al. (2015) discovered intermediate-felsic intrusions rocks that represented the post-collision environment both south and north of the Bangong-Nujiang suture belt, which formed at 75.9–90.7 Ma. These data show that the closure of the Bangong Lake-Nujiang Tethys Ocean may have extended to late Early Cretaceous at approximately 100 Ma (Liu et al., 2014; Li et al., 2015). Therefore, the late Early Cretaceous magma in the Duolong area should not be formed by a collision between Lhasa and Qiangtang terrane. Recall, this paper measured the granodiorite porphyry in the Naruo deposit and found that it belongs to a high potassium calcium alkaline and peraluminous rock series and is relatively enriched in

LREEs and LILEs but low in both HREEs and HFSEs (Fig. 6c,d); in the Ta-Yb, Rb-Y+Nb diagrams, the major intrusive rocks, including those in the Duolong area,lie within the volcanic arc granite field (Fig. 9a,b), which are different from the granite formed in the post-collision environment, and show the characteristics of arc magmas above a subduction zone(Rollinson., 1993; Stolz et al., 1996; Grove et al. 2003). Moreover, in the Th/Ta and Ta/Yb-Th/Yb diagrams (Fig. 9c, d), all of the samples fall into the active continental margin regions. Yet, in the continental margin arc region of the Th-Co-Zr/10 and Th-Sc-Zr/10 diagrams (Fig. 9e, f), which reflects the characteristics of rocks in continental margin arc environments. In addition, the rocks in this area are

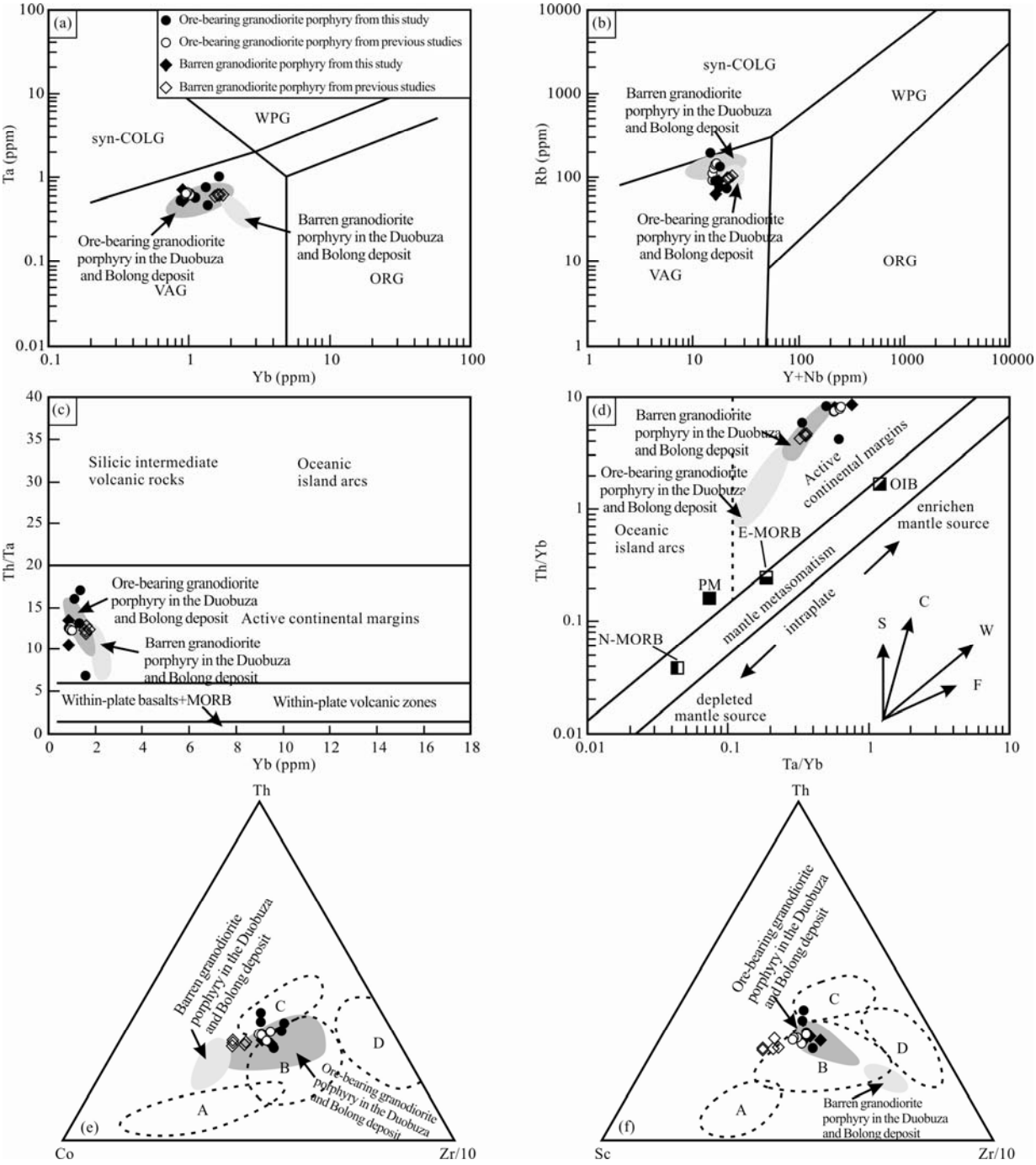

Fig. 9. Geochemical discrimination diagrams of granodiorite porphyry from the Naruo porphyry Cu (Au) deposit.
(a) Ta-Yb diagram (after Pearce et al. 1984); (b) Rb-Y+Nb diagram (after Pearce, 1996); (c) Th/Ta-Yb diagram (after Gorton and Schandl, 2000); (d) Th/Yb-Nb/ Yb diagram (after Pearce, 1983); (e) Th-Co-Zr/10 and (f) Th-Sc-Zr/10 (after Bhatia and Crook. 1986). Tectonic settings: syn-COLG, syn-collisional granites; VAG, volcanic arc granites; WPG, within-plate granites. A, oceanic island arc; B, continental island arc; C, active continental margin; D, passive continental margin.The data for the ore-bearing and barren granodiorite porphyry in the Duobuza and Bolong deposit are from Li et al. (2013); Chen Huaan et al. (2013). The data for the published granodiorite porphyry are from Zhu Xiangping et al. (2015).

granodiorite porphyry+ granite porphyry+andesite (lower Cretaceous Meiriqiecuo group), which are different from intra-ocean arc rocks that are mainly composed of quartz diorite+island arc basalt+andesite (Singer et al., 2005). In contrast to an island arc environment, the porphyry components are slightly acidic (Misra, 2000). In conclusion, the magmatic activity in this area indicated that the formation of the magmatic rocks were closely related to the subduction of the Bangong Lake-Nujiang Tethys Ocean to the south of the Qiangtang terrace, which is similar to the continental margin arc environment of the ocean-continent subduction setting of the Andes metallogenic belt in South America (Högdahl et al., 2008).

6.3 Origin and petrogenesis of magmas

The origin of the magma that is related to the mineralization in the Duolong area has many explanations. Early researchers believed that the magma formed by the partial melting of the shallow crust (Qu Xiaoming et al., 2006, 2012, 2015; Qu et al., 2012; Xin Hongbo et al., 2009) or originated from the melting of an accretionary wedge on the continental margin (Li Guangming et al., 2011; Duan Zhiming et al., 2013).

Based on the diagenesis and mineralization age and geochemical properties of rocks, the above text discusses granodiorite porphyry found in the Duolong areapossessthe characteristics of arc magma above the subduction zone. Early studies showed that arc magma generally originated from the subductionoceanic crustand mantle dehydration or melting (Sillitoe, 1972; Defant and Drummond,1990; Peacock et al., 1994; Yogodzinski et al., 2001)or the melt / fluid metasomatic wedge-shaped mantle zone(Richards, 2003, 2005). The main magmatic rocks in the Doron area are generally rich in silicon and aluminum, high in Sr (395.44–400 ppm), low in Y (10.48 ppm), with adakitic rock characteristics (Defant and Drummond, 1990). In the Y-Sr/Y diagram (Fig. 10a) and the Yb_N-$(La/Yb)_N$ diagram (Fig. 10b), they are mostly located in the transitional region of Adakite and Classical Island arc volcanic rocks, characterized by the end members of both kinds of rocks. Studies proved that when the oceanic crust was subducted to a certain depth, different levels of phase

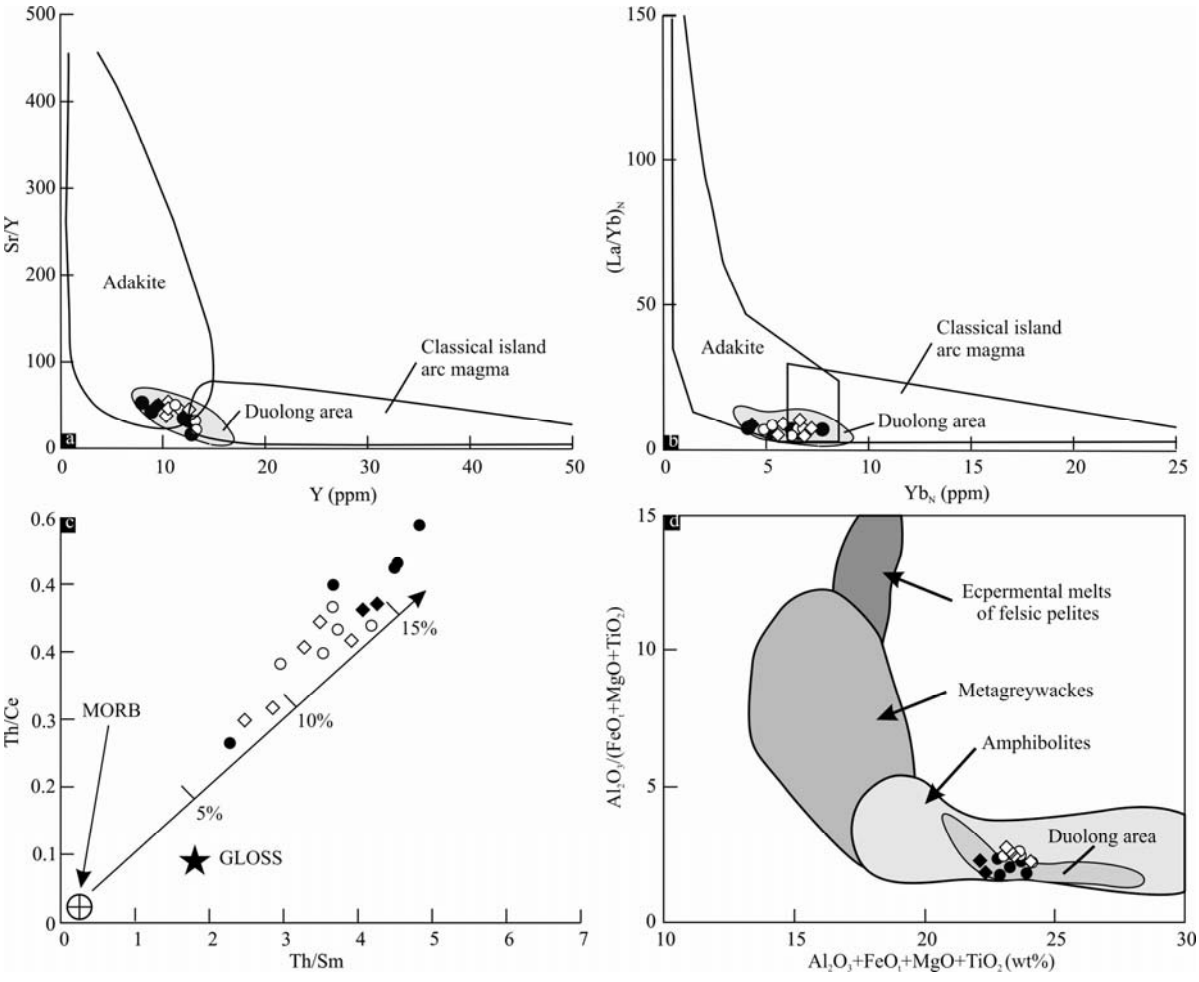

Fig. 10. Discriminant diagrams of source regions of granodiorite porphyry from the Naruo Cu(Au) deposit (after Patiño, 1999). Symbols are as those in Fig. 9.

transition of amphibolite-eclogite occurred, which in turn led to partial melting of the subducted oceanic plateand production of adakitic melt, and became this kind of ideal source region that is aqueous, high in oxygen fugacity, and rich in sulfur magma (Defant and Drummond, 1990; Drummond et al, 1996; Martin et al., 2005). In the Th/Sm-Th/Ce diagram (Fig. 10c), the rock samples in the Dolong area all fall on the subducted sediment curve, showing that nearly 15% of the sediments underwent melting during magma formation (Boztuğ et al., 2007). The weak negative anomalies of Ce also show the characteristics of oceanic sediment addition. However, the depleted Nb, Ta and Ti rocks in the Duolong area similarly shows the characteristics of the components of the rocks with mantle-derived imprints in the subduction zone (Sun and Mcdonough, 1989).Usually, magma originating from the mantle contains higher $Mg^{\#}$, which is typically greater than 50 (Rapp et al., 1999). The moderate $Mg^{\#}$ of granodiorite porphyry in the mining area (ranging from 32.6 to 36.68 ppm) obviously did not originate directly from the mantle. Nevertheless, the melts produced by the partial melting of the subducted oceanic platewere bound to have interacted with the mantle substances when it ascended through the wedge-shaped mantle area. Thesewould result in the mixture between the melt metasomatic mantle wedge or meltsand the mantle-sourced melts (Keleman, 1995; Stern and Kilian, 1996), with the latter often showing higher $Mg^{\#}$ (Kay, 1978; Keleman, 1995). The $Mg^{\#}$ of magmatic rocksin the mining area being less than 40 seems to support the metasomatism of melt/fluidandmantle rocks. In recent years, experimental studies have shown that the equilibrium reaction occurring between the melts, produced by the subductedplate and mantle rocks, would lead to increased content of transitional elements such as Cr, Co, and Ni (Yogodzinski et al., 2001; Xiong et al., 2006). The characteristics of rich Cr (4.78–7.34 ppm), Co (6.05~9.33 ppm), and Ni (2.69–13.19 ppm) in the rocks of the mining area, also confirmed the above inference. In addition, when the depletion of elements such as Nb and Ta appears in rocks, the Y/Yb value and the heavy rare earth distribution pattern can indicate the residual phase of the magma source. The Y/Yb value of this test approached 10 (Y/Yb = 7.21–10.64; average value is 9.26) with the flat-shaped heavy rare earth distribution pattern, indicating that amphibole was the main residual phase of the source region (Sisson, 1994). Also, in the Al_2O_3+FeOT+MgO+TiO_2-Al_2O_3/(FeOT+MgO+TiO_2) source region distinction diagram (Fig. 10d), all samples fall into the amphibolite area, similarly showing that amphibole was the main molten mineral in the source region (Patiño, 1999). More importantly, theresearch obtained relatively uniform positive $\varepsilon Hf(t)$ values of granodiorite porphyry zircon in the Naruo mining area.In the $\varepsilon Hf(t)$ age diagram, the data points invariably fall between the chondrites and depleted mantle and are consistent with the main intrusive rocks in the Duolong area (Fig. 11), showing the characteristics of

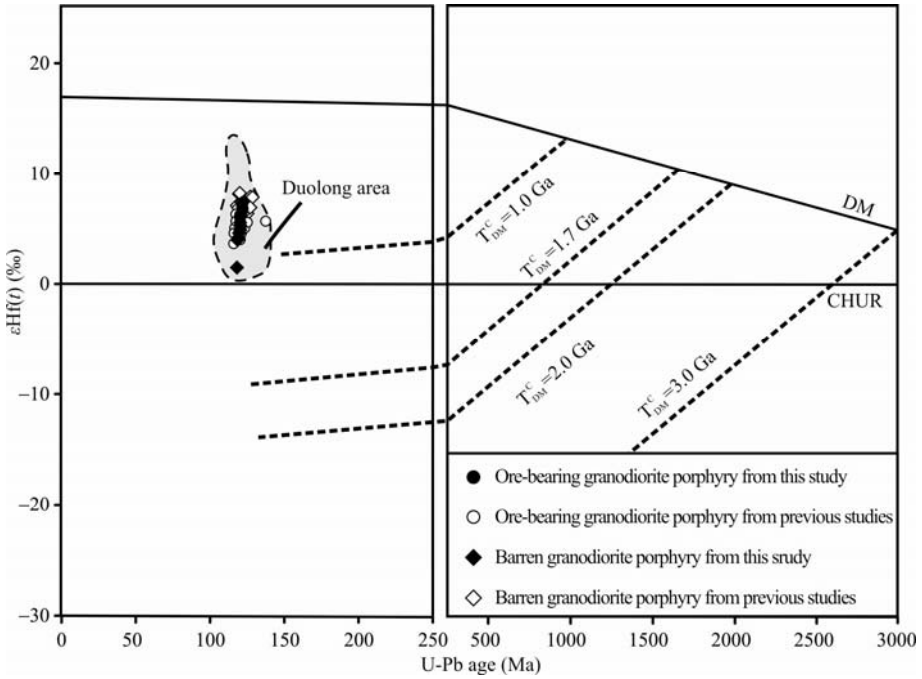

Fig. 11. Plot of $\varepsilon Hf(t)$ versus U-Pb ages of granodiorite porphyry from the Naruo Cu(Au) deposit.

The data for the published granodiorite porphyry are from Zhu Xiangping et al. (2015). The data of Duolong area are from Li et al. (2013) and Chen Huaan et al. (2013).

the addition of mantle source compositions. At the same time, since the crustal model age (TDMC) of granodiorite porphyry is between 707 and 1066 Ma, it reflected the longer detention time of magma in the crust, suggesting the contamination of crust-derived material of different degrees occurred during the magma rising emplacement process. These general characteristics of low $Mg^{\#}$ and high potassium content of these rocks also appears to support the addition of crustal material. Hence, the magmatic formation in the Duolong area and the phase change caused by the subduction of the Bangong Lake-Nujiang Tethyan oceanic crust to 50–70 km depth further resulted in arc magma generated by the melt metasomatic wedge mantle produced by dehydration of minerals like amphiboles. In its ascending process, the magma also experienced varying degrees of crustal contamination.

6.4 Geodynamic processes for the deposit formation

The Early Cretaceous magmatic arc in southern Qiangtang, including the Duolong deposit, is considered to be the product of the northward subduction of the Bangong Lake-Nujiang Tethys Ocean (Liao Liugen et al., 2005; Cao Shenhua et al., 2006; Geng Quanru et al., 2011; Qu et al., 2012; Li et al., 2014) and the slab entering the mantle beneath the Qiangtong terrane in the Early Cretaceous (124–104 Ma). The subducting slab could not melt because its temperature was lower than the surrounding environment. However, because of friction between the slabs and high-temperature heat transfer through the mantle as well as the gradual increase in the hydrostatic pressure in the rocks with increasing depth, phase changes occurred in the sediment of the oceanic crust, which lead to the dehydration of amphibole-like minerals and the appearance of an independent fluid phase. This fluid entered the hot upper mantle wedge through diffusion and metasomatism, which partially melted the hot but dehydrated mantle rocks that originally could not be melted by lowering their melting point and produced arc magmas (Fig. 12a). As a result, these magmas have weak negative Ce anomalies (White and Patchett, 1984), and the high field strength elements remained because of metasomatism between the mantle wedge and the fluid from the dehydration of the subducting slab. At the same time, the addition of water reduced the viscosity of the mantle and triggered convection in the mantle wedge, which rapidly thinned a large area of the lithosphere above the mantle wedge and reduced its resistance to the upwelling magmas. The magmas that were produced by partial melting of the mantle wedge migrated upward because of the difference in density with the mantle rocks. The rising magmas experienced melting, assimilation, storage, and homogenization (Hildreth and Moorbath, 1988). Because they were contaminated by crustal materials, the magmas contained some of the characteristics of the crustal sources, such as the low Nb and Ta contents (Dungan et al., 1986; Foley, 1992), and thus formed intermediate-felsic magmas that were enriched with water, metals, and sulfur. The magmas formed a magma chamber in the shallow crust and separated fluids with high oxygen fugacity after condensation and crystallization, which filled and metasomatized the feldspar quartz porphyry and the sandstone near the contact zone. Sulfides were deposited because of the precipitation and the decrease in temperature and pressure, which ultimately formed the porphyry-epithermal Cu(Au) deposit in the Duolong area (Fig. 12b).

7 Conclusions

(1) The zircon U-Pb ages of the granodiorite porphyry in the Naruo deposit that were measured in this study range from 119.32 Ma to 120.63 Ma, which is consistent with the other porphyry-epithermal Cu(Au) deposits in Duolong area. The ages of all of these deposits are approximately 120 Ma, indicating that large-scale magmatic activity during the Early Cretaceous (124–114 Ma) was the major factor for the formation of the deposits in this area.

(2) According to the whole-rock geochemistry, these rocks belong to a high potassium calcium alkaline and peraluminous rock series with relatively enriched LREEs and LILEs (e.g., Rb, K, Sr) but low HFREEs and HFSEs (Nb, Ta, Ti, P), which is representative of the continental margin arc environment above the subduction zone where they formed.

(3) The in-situ Hf isotopes suggest that the magma in the Duolong area originated from the Bangong Lake-Nujiang Tethys ocean basin subduction zone and formed by the partial melting of the mantle wedge through the dehydration replacement of amphibole minerals.

Acknowledgements

This research was jointly supported by Public Science and Technology Research Funds Projects (201511017) and assistance from the project team at the Institute of Mineral Resources, Chinese Academy of Geological Sciences, and several engineers of the No. 5 Geological Team of the Tibet Geological Exploration Bureau, including LI Yanbo and WEI Lujie Wei. We also appreciate the financial support for our field and laboratory research from executive manager FENG Daoyong, senior engineer SU Dengkui of the Tibet Jinlong Mining Co., Ltd. Additionally, we thank the editor and the reviewers for their valuable comments.

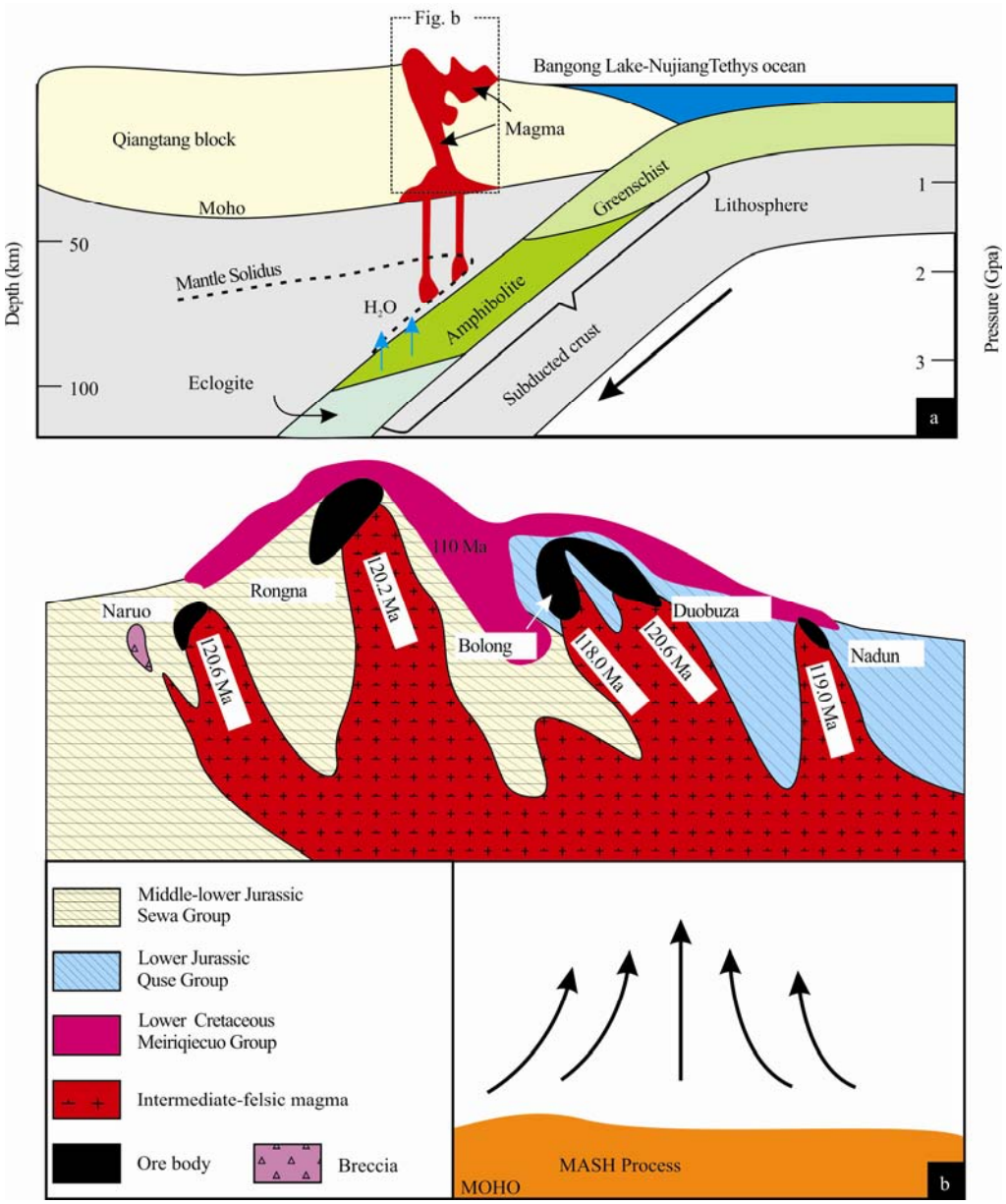

Fig. 12. Geodynamic model for the generation of magma and the formation of the deposit in the Duolong area.
The model of sub-slab is after Manning (2004).

Manuscript received Aug. 20, 2016
accepted Dec. 20, 2016
edited by Fei Hongcai

References

Amelin, Y., Lee, D.C., and Halliday, A.N., 2000. Early–Middle Archaean crustal evolution deduced from Lu–Hf and U–Pb isotopic studies of single zircon grains. *Geochimica et Cosmochimica Acta*, 64 (24): 4205–4225.

Andersen, T., 2002. Correction of common Lead in U–Pb analyses that do not report 204Pb. Chemical Geology, 192: 59–79.

Belousova, E., Suzanne, G.W., and Fisher, Y., 2002. Igneous zircon: trace element composition as an indicator of source rock type. *Contributions to Mineralogy Petrology*, 143: 602–622.

Bhatia, M.R., and Crook, K.A.W., 1986. Trace element characteristics of graywackes and tectonic setting discrimination of sedimentary basins. *Contributions to Mineralogy and Petrology*, 92: 181–193.

Bouvier, A., Jeffrey, D., and Vervoort, P., 2008. The Lu-Hf and Sm-Nd isotopic composition of CHUR: Constraints from unequilibrated chondrites and implications for the bulk composition of Terrestrial planets. *Earth and Planetary Scinenee Letters*, 273(1–2): 48–57.

Boynton, W.V., 1984. Cosmochemistry of the rare earth elements: Meteorite studies. *Rare Earth Element Geochemistry*, 63–114.

Boztuğ, D., Harlavan, Y., Arehart, G.B., Satird, M., Avci, N., 2007. K-Ar age, Whole-rock and isotope geochemistry of A-

Type granitoids in the Divrigi Sivas Region, eastern-central Anatolia, Tuikey. *Lithos*, 97(1): 1931–218.

Cao Shenghua, Deng Shiquan, Xiao Zhijian and Liao Liugen, 2006.The Archipelagic arc tectonic evolution of the Meso–Tethys in the western part of the Bangong Lake–Nujiang suture zone. *Sedimentary Geology and Tethyan Geology*, 26 (4): 25–32(in Chinese with English abstract).

Chen Huaan, Zhu Xiangping, Ma Dongfang, Huang Hanxiao, Li Guangming, Li Yubin, Li Yuchang, Wei Lujie and Liu Zhaoqiang, 2013. Geochronology and geochemistry of the Bolong porphyry Cu–Au deposit, Tibet and its mineralizing significance. *Acta Geologica Sinica*, 87(10): 1593–1611 (in Chinese with English abstract).

Cooke, D.R., Hollings, P., and Walsh, J.L., 2005. Giant porphyry deposits: Characteristics, distribution, and tectonic controls. *Economic Geology*, 100(5): 801–818.

Cui Ning, Xing Shuwen, Xiao Keyan, and Ding Jianhua, 2016.Geological characteristics and resource potential analysis of the Banggong-Nujiang Cu-Au-Fe-Li metallogenic belt. *Acta Geologica Sinica*, 90(7): 1623–1635 (in Chinese with English abstract).

Defant, M.J., and Drummond, M.S., 1990. Derivation of some modern arc magmas by melting of young subducted lithosphere. *Nature*, 34: 662–665.

Drummond, M.S., Defant, M.J., and Kepezhinskas, P.K., 1996. Petrogenesis of slab-derived trondhjemite–tonalite –dacite / adakite magmas. *Earth and Environmental Science Transactions of the Royal Society of Edinburgh*, 87: 205-215.

Duan Zhiming, Li Guangming, Zhang Hui and Duan Yaoyao, 2013. The formation and its significance of Late Triassic–Jurassic accretionary complexes and constraints on metallogenic and geological settings in Duolong porphyry copper gold ore concentration area, northern Bangong Co-Nujiang suture zone, Tibet. *Geological Bulletin of China*, 32 (5): 742–750 (in Chinese with English abstract).

Dungan, M.A., Lindstrom, M.M., McMillan, N.J., Moorbath, S., Hoefs, J., and Haskin, L.A., 1986. Open system magmatic evolution of the Taos Plateau volcanic field, Northern New Mexico: 1. The petrology and geochemistry of the Servilleta basalt. *Journal of Geophysical Research*. Part B, Solid Earth, 91: 5999–6028.

Eliopoulos, D.G., Eliopoulos, M.D., and Zelyaskova, P.M., 2014. Critical factors controlling Pd and Pt potential in porphyry Cu-Au deposits: evidence from the Balkan Peninsula. *Geosciences*, 4(1): 31–49.

Fang Xiang, Tang Juxing, Song Yang, Yang Chao, Ding Shuai, Wang Yiyun, Wang Qin, Sun Xingguo, Li Yubin, Wei Lujie, Zhang Zhi, Yang Huanhuan, Gao Ke and Tang Pan, 2015. Formation epoch of the South Tiegelong supelarge epithermal Cu (Au–Ag) deposit in Tibet and its geological implications. *Acta Geoscientica Sinica*, 36(2): 168–176 (in Chinese with English abstract).

Foley, S.F., 1992. Petrological characteristics of the source components of potassic magmas: Geochemical and Experimental Constraints. *Lithos*, 28: 178–204.

Fu Jiajun, Ding Lin, Xu Qiang, Cai Fulong, Yue Yahui and Guo Yu, 2015. Zircon U–Pb geochronology and Hf isotopic composition of the Cretaceous volcanic rocks and constraint of the collision age of Bangong–Nujiang Suture Zone in Dongco area, Gaize, Tibet. *Chinese Journal of Geology*, 50 (1): 182–202 (in Chinese with English abstract)

Geng Quanru, Pan Guitang, Wang Liquan, Peng Zhimin and Zhang Zhang, 2011.Tethyan evolution and metallogenic geological background of the Bangong Co–Nujiang belt and the Oiangtang massif in Tibet. *Geological Bulletin of China*, 30(8): 1261–1274 (in Chinese with English abstract).

Gorton, M.P., and Schandl, E.S., 2000. From continents to island arcs: A geochemical index of tectonic setting for arc–related and within–plate felsic to intermediate volcanic rocks. *The Canadian Mineralogist*, 38: 1065–1073.

Grove, T.L., Elkins Tanton, L.T., Parman, S.W., Chatterjee, N., Muntener, O., and Gaetani, G.A., 2003. Fractional crystallization and mantle-melting controls on calc-alkaline differentiation trends. *Contributions to Mineralogy and Petrology*, 145: 515–533.

Gustafson, L.B., 1978. Some major factors of porphyry copper genesis. *Economic Geology*, 73(5): 600–607.

Guynn, J.H., Kapp, P., Pullen, A., Heizle, M., Gehrels, G., and Ding, L., 2006. Tibetan basement rocks near Amdo reveal "missing" Mesozoic tectonism along the Bangong suture, central Tibet. *Geology*, 34(6): 505–508.

Halter, W., Heinrich, C., and Pettke, T., 2005. Magma evolution and the formation of porphyry Cu-Au ore fluids: Evidence from silicate and sulfide melt inclusions. *Mineral Deposita*, 39 (8): 845–863.

Hildreth, W., and Moorbath, S., 1988. Crustal contributions to arc magmatism in the andes of central Chile. *Contributions to Mineralogy and Petrology*, 98: 455–489.

Högdahl, K., Sjöström, H., Andersson, U.B., and Martin, A., 2008. Continental margin magmatism and migmatisation in the West-Central Fennoscandian Shield. *Lithos*, 102(3): 435–459.

Hou Kejun, Li Yanhe, Zou Tianren, Qu Xiaoming, Shi Yuruo and Xie Guiqing, 2007. Laser Ablation–MC–ICP–MS technique for Hf isotope microanalysis of zircon and its geological applications. *Acta Petrologlca Sinica*, 23(10): 2595–2604(in Chinese with English abstract).

Hou, Z.Q., Ma H.W., Khin, Z., Zhang, Y.Q., Wang, M.J., Wang, Z., Pan, G.T., and Tang, R.L., 2003. The Himalayan Yulong porphyry copper belt: Product of large-scale strike-slip faulting in eastern Tibet. *Economic Geology*, 98(1): 125–145.

Hou, Z.Q., Gao, Y.F., Qu, X.M., Rui, Z.Y., and Mo, X.X., 2004. Origin of adakitic intrusives generated during mid-Miocene east–west extension in southern Tibet. *Earth and Planetary Science Letters*, 220: 139–155.

Hou Z.Q., Xie Y.L., Xu W.Y., Li Y.Q., Zhu X.K., Zaw, K., Beaudoin, G., Rui Z.Y., Hang W., and Luobu C.R., 2007. Yulong deposit, eastern Tibet: A high–sulfidation Cu–Au porphyry copper deposit in the eastern Indo–Asian collision zone. *International Geology Review*, 49(3): 235–258.

Hou, Z.Q., Yang, Z.M., Qu X.M., Meng, X.J., Li, Z.Q., Beaudoin, G., Rui, Z.Y., Gao, Y.F., and Zaw, K., 2009. The Miocene Gangdese porphyry copper belt generated during post-collisional extension in the Tibetan Orogen. *Ore Geology Reviews*, 36(1–3): 25–51.

Hou, Z.Q., Zheng, Y.C., Yang, Z.M., Rui, Z.Y., Zhao, Z.D, Jiang S.H., Qu, X.M., and Sun ,Q.Z., 2013. Contribution of mantle components within juvenile lower-crust to collisional zone porphyry Cu systems in Tibet. *Mineralium Deposita*, 48(2): 173–192.

Jiang, Y.H., Jiang, S.Y., Dai, B.Z., and Ling, H.F., 2008. Discrimination of ore-bearing and barren porphyries in

the Yulong porphyry copper ore belt, Eastern Tibet. *International Geology Review*, 50(6): 583–595.

Kay, R.W.J., 1978. Aleutian magnesium andesites,melts from subducted pacific oceanic crust. *Journal of Volcanology and Geothermal Research*, 4:117–132.

Kapp, P., Yin, A., Manning, C.E., Harrison, T.M., Taylor, M.H., Ding, L., and Guo, J.H., 2003. Tectonic evolution of the early Mesozoic blueschistbearing Qiangtang metamorphic belt, central Tibet. *Tectonics*, 22(4): 312–323.

Keleman, B.P., 1995. Genesis of High Mg# Andesites and the Continental Crust. *Contributions to Mineralogy and Petrology*, 120: 1–19.

Kesler, S.E., and Wilkinson, B.H., 2008. Earth's copper resources estimated from tectonic diffusion of porphyry copper deposits. *Geology*, 36(3): 255–258.

Li Dewei, 2008. Three–stage tectonic evolution and metallogenic evolution in the Qinghai–Tibet Plateau and its adjacent area. *Earth Science–Journal of China University of Geosciences*, 33 (6): 723–742 (in Chinese with English abstract).

Li Guangming, Duan Zhiming, Liu Bo, Zhang Hui, Dong Suiliang and Zhang Li, 2011. The discovery of Jurassic accretionary complexes in Duolong area, northern Bangong Co–Nujiang suture zone, Tibet, and its geologic significance. *Geological Bulletin of China*, 30(8): 1256–1260 (in Chinese with English abstract).

Li, G.M., Li, J.X., Qin, K.Z., Duo, J., Zhang, T.P., Xiao, B., and Zhao, J.X., 2012. Geology and hydrothermal alteration of the Duobuza gold-rich porphyry copper district in the Bangongco metallogenetic belt, northwestern Tibet. *Resource Geology*, 62 (1): 99–118.

Li Guangming, Zhang Xianan, Qin Kezhang, Sun Xingguo, Zhao Junxing, Yin Xianbo, Li Jinxiang and Yuan Huashan, 2015. The telescoped porphyry–high sulfidation epithermal Cu(–Au) mineralization of Rongna deposit in Duolong ore cluster at the southern margin of Qiangtang terrane, central Tibet: integrated evidence from geology, hydrothermal alteration and sulfide assemblages. *Acta Petrologica Sinica*, 31(8): 2307–2324 (in Chinese with English abstract).

Li Jinxiang, Li Guangming, Qin Kezhang and Xiao Bo, 2008. Geochemistry of porphyries and volcanic rocks and ore forming geochronology of Duobuza gold–rich porphyry copper deposit in Bangonghu belt: constraints on metallogenic tectonic settings. *Acta Petrologica Sinica*, 24(3): 531–543(in Chinese with English abstract).

Li, J.X., Li, G.M., Qin, K.Z., Xiao, B., Chen, L., and Zhao, J.X., 2011a. Mineralogy and mineral chemistry of the Cretaceous Duolong gold–rich porphyry copper deposit in the Bangongco arc, northern Tibet. *Resource Geology*, 62(1): 19–41.

Li J.X., Qin K.Z., Li G.M., Xiao B., Zhao J.X., and Chen L., 2011b. Magmatic–hydrothermal evolution of the Cretaceous Duolong gold–rich porphyry copper deposit in the Bangongco metallogenic belt, Tibet: Evidence from U–Pb and 40Ar/39Ar geochronology. *Journal of Asian Earth Sciences,* 41(6): 525–536.

Li, J.X., Qin, K.Z., Li, G.M., Zhao, J.X., Cao, M.J., and Chen L., 2013. Petrogenesis of ore–bearing porphyries from the Duolong porphyry Cu–Au deposit, central Tibet: evidence from U–Pb geochronology, petrochemistry and Sr–Nd–Hf–O isotope characteristics. *Lithos*, 160–161: 216–227.

Li, J.X., Qin, K.Z., Li, G.M., Richards, J.P., Zhao, J.X., and Cao, M.J., 2014. Geochronology, geochemistry, and zircon Hf isotopic compositions of Mesozoic intermediate–felsic intrusions in central Tibet: petrogenetic and tectonic implications. *Lithos*, 198–199: 77–91.

Li, Y.L., He, J., Wang, C.S., Han, Z.P., Ma, P.F., Xu, M., and Du, K.Y., 2015. Cretaceous volcanic rocks in south Qiangtang Terrane: Products of northward subduction of the Bangong–Nujiang ocean? *Journal of Asian Earth Sciences*, 104: 69–83.

Liang, H.Y., Campbell, I.H., Allen, C., Sun, W.D., Liu, C.Q., Yu, H.X., Xie, Y.W., and Zhang, Y.Q., 2006. Zircon Ce^{4+}/Ce^{3+} ratios and ages for Yulong ore-bearing porphyries in eastern Tibet. *Mineralium Deposita*, 4l(2): 152–159.

Liang, H.Y., Sun, W.D., Su, W.C., and Zartmanet, R.E., 2009.Porphyry copper-gold mineralization at YuLong, China, promoted by decreasing redox potential during magnetite alteration. *Economic Geology*, 104(4): 587–596.

Liao Liugen, Cao Shenghua, Xiao Yebin, Ouyang Kegui, Hu Zhaorong and Feng Guosheng, 2005. The archipelagic are tectonic evolution of the Meso–Tethys in the western part of the Bangong Lake–Nujiang suture zone. *Sedimentary Geology and Tethyan Geology*, 25(1–2): 163–170 (in Chinese with English abstract).

Liu, D.L., Huang, Q.S., Fan, S.Q., Zhang, L.Y., Shi, R.D., and Ding, L., 2014. Subduction of the Bangong–Nujiang ocean: constraints from granites in the Bangong Co area, Tibet. *Geological Journal*, 49: 188–206.

Liu, S., Hu, R.Z., Gao, S., Feng, C.X., Coulson, I.M, Feng, G.Y., Qi, Y.Q., Yang, Y.H., Yang, C.G., and Tang, L., 2012. U–Pb zircon age, geochemical and Sr–Nd isotopic data as constraints on the petrogenesis and emplacement time of andesites from Gerze, southern Qiangtang block, northern Tibet. *Journal of Asian Earth Sciences*, 45(2): 150–161.

Logan, J.M., and Mihalynuk, M.G., 2014. Tectonic controls on early mesozoic paired alkaline porphyry deposit belts(Cu–Au ± Ag–Pt–Pd–Mo) within the Canadian Cordillera. *Economic Geology*, 109(4): 827–858.

Ludwig, K.R., 2003. *Isoplot/Ex version 3.0 a geochronological toolkit for Microsoft excel*. Berkeley Geochronology Centre Special Publication, 4: 1–70.

Manning, C.E., 2004. The chemistry of subduction–zone fluids. *Earth and Planetary Science Letters*, 223(1–2): 1–16.

Martin, H., Smithies, R.H., Rapp, R., Moyen, J.F., and Champion, D., 2005. An overview of adakite, tonalite trondhjemite granodiorite (TTG) and sanukitoid: relationships and some implications for crustal evolution. *Lithos*, 79: 1–24.

Misra, K.C., 2000.*Understanding mineral deposits*. Kluwer Academic Publishers, 353–413.

Matte, P., Tapponnier, P., Arnaud, N., Bourjot, L., Avouac, J.P., Vidal, P., Liu, Q., Pan, Y., and Wang, Y., 1996. Tectonics of western Tibet, between the Tarim and the Indus. *Earth and Planetary Science Letters*, 142(3–4): 311–330.

Patiño, D.A.E., 1999. What do experiments tell us about the relative contributions of crust and mantle to the origin of granitic magmas? *Geological Society, London, Special Publications*, 168: 55–75.

Peacock, S.M., Rusher, T., and Thompson, A.B., 1994. Partial melting of subducting oceanic crust. *Earth and Planetary Science Letters*, 121: 227–244.

Pearce, J.A., 1983. Role of the sub–continental lithosphere in magma genesis at active continental margins. In: Hawkeswrth, C.J., and Norry, M.J. (eds.), *Continental basalts and mantle xenoliths: Nantwich, Shiva*, 230–249.

Pearce, J.A., Harris, N.B.W., and Tindle, A.G., 1984. Trace element discrimination diagrams for the tectonic interpretation of granitic rocks. *Journal of Petrology*, 25(4): 956–983.

Pearce, J.A., 1996. Source and settings of granitic rocks. *Episodes*, 19(4): 120–125.

Peccerillo, A., and Taylor, S.R., 1976. Geochemistry of eocene calc-alkaline volcanic rocks from the Kastamonu area, northern Turkey. *Contributions to Mineralogy and Petrology*, 58: 63–81.

Qu Huanhuan and Sun Maoyu, 2016. Where were the metal, sulfur and water from in the postcollisional porphyry Cu deposit at Qulong in south Tibet? *Acta Geologica Sinica* (English edition), 90(2): 753–754.

Qu Xiaoming and Xin Hongbo, 2006. Age and tectonic environment of the Bangong Co porphyry copper belt in western Tibet, China. *Geological Bulletin of China*, 25(7): 792–799 (in Chinese with English abstract).

Qu Xiaoming, Wang Ruijiang, Xin Hongbo, Zhao Yuanyi and Fan Xingtao, 2009. Geochronology and geochemistry of igneous rock related to the subduction of the Tethys oceanic plate along the Bangong Lake arc zone, the western Tibetan plateau. *Geochimica*, 38(6): 523–535 (in Chinese with English abstract).

Qu Xiaoming, Wang Ruijiang, Dai Jingjing, Li Youguo, Qi Xun, Xin Hongbo, Song Yang and Du Dedao, 2012. Discovery of Xiongmei porphyry copper deposit in middle segment of Bangonghu–Nujiang suture zone and its significance. *Mineral Deposits*, 31(1): 1–12 (in Chinese with English abstract).

Qu, X.M., Wang, R.J., Xin, H.B., Jiang, J.H., and Chen, H., 2012. Age and petrogenesis of A–type granites in the middle segment of the Bangonghu–Nujiang suture, Tibetan Plateau. *Lithos*, 146–147: 264–275.

Qu Xiaoming, Fan Shufang, Ma Xudong and Song Yang, 2015. Post–collisional copper ore deposits along Bangong Co–Nujiang metallogenic belt, Tibetan Plateau. *Mineral Deposits*, 34(3): 431–448 (in Chinese with English abstract).

Rapp, R.P., Shimizu, N., Norman, M.D., and Applegate, G.S., 1999. Reaction betweens lab derived melts and peridotite in the mantle wedge: experimental constraints at 3.8 GPa. *Chemical Geology*, 160: 335–356.

Richards, J.P., 2003. Tectono-magmatic precursors for porphyry Cu-(Mo-Au) deposit formation. *Economic Geology*, 98(8): 1515–1533.

Richards, J.P., 2005. Cumulative factors in the generation of giant calc-alkaline porphyry Cu deposits. In: Porter, T.M. (ed.), *Super Porphyry Copper & Gold Deposits*. PGC Publishing, 1:7–25.

Rollinson, H.P., 1993. *Using Geochemical Date: Evaluation, Presentation, Interpretation*. New York: Longman Publishing Group, 174–206.

Schwab, M., Ratschbacher, L., Siebel, W., McWilliams, M., Minaev, V., Lutkov, V., Chen, F., Stanek, K., Nelson, B., Frisch, W., and Wooden, J. L. 2004. Assembly of the Pamirs: age and origin of magmatic belts from the southern Tien Shan to the southern Pamirs and their relation to Tibet. *Tectonics*, 23(4): 1–31.

Seedorff, E., Dilles, J., Proffett, Jr.J., Einaudi, M., Zurcher, L., Stavast, W., Johnson, D., and Barton, M., 2005. Porphyry deposits: Characteristics and origin of hypogene features. *Economic Geology 100th Anniversary*, 251–298.

She Hongquan, Li Jinwen, Ma Dongfang, Li Guangming, Zhang Dequan, Feng Chengyou, Qu Wenjun and Pan Guitang, 2009. Molybdenite Re-Os and SHRIMP zircon U–Pb dating of Duobuza porphyry copper deposit in Tibet and its geological implications. *Mineral Deposits*, 28(6): 737–746 (in Chinese with English abstract).

Shi Rendeng, 2007. SHRIMP dating of the Bangong Lake SSZ–type ophiolite: constraints on the closure time of ocean in the Bangong Lake–Nujiang River, northwestern Tibet. *Chinese Science Bulletin*, 52(7): 936–941.

Sillitoe, R.H., 1972. A plate tectonic model for the origin of porphyry copper deposits. *Economic Geology*, 67:184-197.

Sillitoe, R.H., 1979. Some thoughts on gold-rich porphyry copper deposits. *Mineral Deposita*, 14(2): 161–174.

Sillitoe, R.H., and Perelló, J., 2005. Andean copper province: tectonomagmatic settings, deposit types, metallogeny, exploration, and discovery. *Economic Geology 100th Anniversary Volume*, 845−890.

Sillitoe, R.H., 2010. Porphyry copper systems. *Economic Geology*, 105(1): 3–41.

Sinclair, W.D., 2007. Porphyry deposits. In: Goodfellow, W.D. (ed.), *Mineral Deposits of Canada: A synthesis of major deposit types, district metallogeny, the evolution of geological provinces and exploration methods*. Geological Association of Canada, Mineral Deposits Division, Special Publication, 5: 223–243.

Singer, D.A., 1995. World class base and precious metal deposits–a quantitative analysis. *Economic Geology*, 90(1): 88–104.

Singer, D.A., Menzie, W.D., and Berger, B.R., 2005. Porphyry copper deposit density. *Economic Geology*, 100: 491–514.

Singer, D.A., 2008. Mineral deposit densities for estimating mineral resources. *Mathematical Geosciences*, 40 (1): 33–46.

Sisson, T.W., 1994. Hornblende-melt trace-element partitioning measured by ion Microprobe. *Chemical Geology*, 117(1): 331–344.

Söderlund, U., Patchett, P.J., Vervoort, J.D., and Isachsen, C.E., 2004. The 176Lu decay constant determined by Lu–Hf and U–Pb isotope systematics of precambrian marie intrusions. *Earth and Planetary Science Letters*, 219(3–4): 311–324.

Stern, C.R., and Kilian, R., 1996. Role of the subducted slab, mantle wedge and continental crust in the generation of Adakites from the Andean Austral volcanic zone. *Contributions to Mineralogy and Petrology*, 123: 263–281.

Stolz, A.J., Jochum, K.P., Spettel, B., and Hofmann, A.W., 1996. Fluid and melt–related enrichment in the subarc mantle: Evidence from Nb/Ta variations in island arc basalts. *Geology*, 24: 587–590.

Sun, S.S., and McDonough, W., 1989. Chemical and isotopic systematics of oceanic basalts: Implications for mantle composition and processes. *Geological Society*, 42: 313–345.

Sun, W.D., Liang, H.Y., Ling, M.X., Zhan, M.Z., Ding X., Zhang, H., Yang, X.Y., Li, Y.L., Ireland, T.R., Wei Q.R., and Fan, W.M., 2013. The link between reduced porphyry copper deposits and oxidized magmas. *Geochimica et Cosmochimica Acta*, 103: 263–275.

Sun, W.D., Hang, R.F., Li, H., Hu, Y.B., Zhang, C.C., Sun, S.J., Zhang, L.P., Ding, X., Li, C.Y., Zartman, R.E., and Ling, M.X., 2015. Porphyry deposits and oxidized magmas. *Ore Geology Reviews*, 65: 97–131.

Tang Juxing, Sun Xingguo, Ding Shuai, Wang Qin, Wang Yiyun, Yang Chao, Chen Hongqi, Li Yubin, Li Yaobo, Wei

Lujie, Zhang Zhi, Song Junlong, Yang Huanhuan, Duan Jilin, Gao Ke, Fang Xiangang and Tan Jiangyun, 2014. Discovery of the epithermal deposit of Cu (Au–Ag) in the Duolong ore concentrating area, Tibet. *Acta Geoscientica Sinica*, 35(1): 6–10 (in Chinese with English abstract).

Tang, J.X., Lang, X.H, Xie, F.W, Gao, Y.M., Li, Z.J., Huang, Y., Ding, F., Yang, H.H., Zhang, L., Wang, Q., and Zhou, Y., 2015. Geological characteristics and genesis of the jurassic No. I porphyry Cu–Au deposit in the Xiongcun district, Gangdese porphyry copper belt, Tibet. *Ore Geology Reviews*, 70: 438–456.

Wang Qin, Tang Juxing, Fang Xiang, Lin Bin, Song Yang, Wang Yiyun, Yang Huanhuan, Yang Chao, Li Yubin, Wei Lujie, Feng Jun and Li Li, 2015. Petrogenetic setting of andsites in Rongna ore block, Tiegelong Cu (Au–Ag) deposit, Duolong ore concentration area, Tibet: evidence from zircon U–Pb LA–ICP–MS dating and petrogeochemistry of andsites. *Geology in China*, 42(5): 1324–1336 (in Chinese with English abstract).

White, W.M., and Patchett, J., 1984. Hf–Nd–Sr isotopes and incompatible element abundances in island arcs: implications for magma origins and crust–mantle evolution. *Earth and Planetary Science Letters*, 67: 167–185.

Xin Hongbo, Qu Xiaoming, Wang Ruijiang, Liu Hongfei, Zhao Yuanyi and Huang Wei, 2009. Geochemistry and Pb, Sr, Nd isotopic features of ore-bearing porphyries in Bangong Lake porphyry copper belt, Western Tibet. *Mineral Deposits*, 28(6): 785–792 (in Chinese with English abstract).

Xiong, X.L., Xia, B., Xu, J.F., Niu, H.C., and Xiao, W.S., 2006. Nadepletion in modern adakites via melt/rock reaction within the sub-arc mantle. *Chemical Geology*, 229: 273–292.

Yang Chao, Tang Juxing, Wang Yiyun, Yang Huanhuan, Wang Qin, Sun Xingguo, Feng Jun, Yin Xianbo, Ding Shuai, Fang Xiang, Zhang Zhi and Li Yanbo, 2014. Fluid and geological characteristics researches of southern Tiegelong epithermal porphyry Cu–Au deposit in Tibet. *Mineral Deposits*, 33(6): 1287–1305 (in Chinese with English abstract).

Yin, A., and Harrison, T.M., 2000. Geological evolution of the Himalayan–Tibetan orogen. *Annual Review of Earth and Planetary Sciences*, 28: 211–280.

Yogodzinski, G.M., Lees, J.M., Churikova, T.G., Dorendorf, F., Woeerner, G., and Volynets, O.N., 2001.Geochemical evidence for the melting of subducting oceanic lithosphere at plate rdges. *Nature*, 409: 500–504.

Zimmerman, A., Stein, H.J., Hannah, J.L., Koželj, D., Bogdanov, K., and Berza, T., 2008.Tectonic configuration of the Apuseni–Banat–Timok–Srednagorie belt, Balkans–South Carpathians, constrained by high precision Re-Os molybdenite ages. *Mineral Deposita*, 43(1): 1−21.

Zhang Shuo, Shi Hongfei, Hao Haijian, Li Dewei, Lin Yan and Feng Minxuan, 2014. Geochronilogy, geochemistry and tectonic significanse of Late Cretaceous adakites in Bangong Lake, Tibet. *Earth Science–Journal of China University of Geosciences*, 39(5): 509–524 (in Chinese with English abstract).

Zheng, Y.Y, Sun, X., Gao, S.B, Wu, S., Xu, J., Jiang, J.S, Chen, X., Zhao, Z.Y., and Liu, Y., 2015. Metallogenesis and the minerogenetic series in the Gangdese polymetallic copper belt. *Journal of Asian Earth Sciences*, 103: 23–39.

Zhou Jinsheng, Meng Xiangjin, Zang Wenshuan, Yang Zhusen, Xu Yutao, and Zhang Xiong, 2013. Zircon U–Pb geochronology and trace element geochemistry of the ore–bearing porphyry in Qingcaoshan porphyry Cu–Au deposit, Tibet, and its geological significance. *Acta Petrologica Sinica*, 29(11): 3755–3766 (in Chinese with English abstract).

Zhou Xiong, Fei Guangchun, Zhou Yu, Wen Chunqi, Zhang Yi and Yue Xiangyuan, 2015. Chronology and crust-mantle mixing of ore-forming porphyry of the Bangongco: evidence from zircon U-Pb age and Hf isotopes of the Naruo porphyry copper-gold deposit. *Acta Geologica Sinica* (English Edition), 89(1): 217–228.

Zhu Dicheng, Pan Guitang, Mo Xuanxue, Wang Liquan, Zhao Zhidan, Liao Zhongli, Geng Quanru and Dong Guochen, 2006. Identification for the Mesozoic OIB–type basalts in Central Qinghai–Tibetan Plateau: geochronology, geochemistry and their tectonic setting. *Acta Geologica Sinica*, 80(9): 1312–1328 (in Chinese with English abstract).

Zhu Xiangping, Chen Huaan, Liu Hongfei, Ma Dongfang, Li Guangming, Zhang Hong, Liu Zhaoqiang and Wei Lujie, 2015. Geochronology and geochemistry of porphyries from the Naruo porphyry copper deposit, Tibet and their metallogenic significance. *Acta Geologica Sinica*, 89(1): 109–128 (in Chinese with English abstract).

Zhu, X.P., Li, G.M., Chen, H.A., Ma, D.F., and Huang, H.X., 2015. Zircon U–Pb, molybdenite Re–Os and K–feldspar $^{40}Ar/^{39}Ar$ dating of the Bolong porphyry Cu–Au deposit, Tibet, China. *Resource Geology*, 65(2): 122–135.

About the first author

DING Shuai, male, born in 1987 in Ziyang City, Sichuan Province, PhD, College of Earth Sciences, Chengdu University of Technology, Chengdu 610059, China. He is now interested in the study on metallogeny. E-mail: 7826287282qq.com.Tel: 15882183994.